Doctoral Dissertations

Graduate School

Spring 2011

Development of approximating functions to model and predict the properties of fresh and hardened fly ash-based geopolymer concrete

Eleazar Ivan Diaz Loya

DEVELOPMENT OF APPROXIMATING FUNCTIONS TO MODEL AND PREDICT THE PROPERTIES OF FRESH AND HARDENED FLY ASH-BASED GEOPOLYMER CONCRETE

by

Eleazar Iván Díaz Loya, B.S.

A Dissertation Presented in Partial Fulfillment
of the Requirements for the Degree
Doctor of Philosophy

COLLEGE OF ENGINEERING AND SCIENCE
LOUISIANA TECH UNIVERSITY

May 2011

UMI Number: 3459545

UMI®

Dissertation Publishing

ProQuest®

LOUISIANA TECH UNIVERSITY

THE GRADUATE SCHOOL

03/29/2011
_____
Date

We hereby recommend that the thesis prepared under our supervision

by_ Eleazar Iván Díaz-Loya

entitled_____

DEVELOPMENT OF APPROXIMATING FUNCTIONS TO

MODEL AND PREDICT THE PROPERTIES OF FRESH AND

HARDENED FLY ASH-BASED GEOPOLYMER CONCRETE

be accepted in partial fulfillment of the requirements for the Degree of

Doctor of Philosophy in Engineering

_____
Supervisor of Thesis Research

_____
Head of Department

Engineering
_____
Department

Recommendation concurred in:

Advisory Committee

Approved:

_____
Director of Graduate Studies

_____
Dean of the College

Approved:

_____
Dean of the Graduate School

ABSTRACT

The manuscript presented herein is based on the investigation of the mechanical properties of fly ash-based geopolymer concrete and their link to fly ash (FA) characteristics. A database of 32 FA samples was created. Each FA sample was analyzed in terms of chemical composition, crystallographic properties and particle size distribution. The mechanical performance of geopolymer concrete (GPC) made from each FA sample was evaluated in terms of density, setting time, compressive and flexural strength, static elastic modulus and Poisson's ratio. It is worth mentioning that the author has already published preliminary results of this study (Diaz and Allouche, 2010; Diaz et al. 2010) in peer-reviewed journals. The database was randomly divided into two sets; one consisting of 24 FA samples for model building using linear regression and another consisting of eight FA samples for validation. The first set was analyzed to detect correlations between fly ash characteristics and mechanical properties of GPC. Correlations within the elastic modulus, the compressive and flexural strengths of GPC were also sought and correlations were developed. These equations were tested on the second set of eight FA samples that were not included during the model building process. The results show that the elastic modulus, as well as the compressive and flexural strengths of GPC can be predicted with reasonable accuracy by analyzing the chemical, physical and crystallographic properties of a given FA and following the steps presented in this study.

Additionally, it was also found that the mechanical behavior of GPC is similar to that of ordinary Portland cement (OPC) concrete, suggesting that equations, akin to those given by the American Concrete Institute's Building Code (ACI 318, 2008), could be applied for GPC to determine its flexural strength and static elastic modulus.

APPROVAL FOR SCHOLARLY DISSEMINATION

The author grants to the Prescott Memorial Library of Louisiana Tech University the right to reproduce, by appropriate methods, upon request, any or all portions of this Dissertation. It is understood that "proper request" consists of the agreement, on the part of the requesting party, that said reproduction is for his personal use and that subsequent reproduction will not occur without written approval of the author of this Dissertation. Further, any portions of the Dissertation used in books, papers, and other works must be appropriately referenced to this Dissertation.

Finally, the author of this Dissertation reserves the right to publish freely, in the literature, at any time, any or all portions of this Dissertation.

Author _____
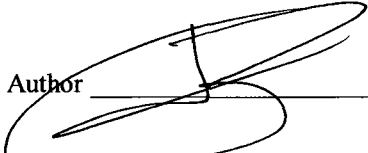
Date _____03/29/2011_____

TABLE OF CONTENTS

LIST OF TABLES

LIST OF FIGURES

LIST OF EQUATIONS

LIST OF SYMBOLS AND ACRONYMS

Analysis of variance	ANOVA
Calcium aluminosilicate hydrates	CASH
Calcium silicate hydrates	CSH
Calculated surface	CS
Coal combustion product	CCP
Compressive strength	f'_c
Density of fresh GPC	w
Elastic modulus	E_c
Elastic net	EN
Environmental Protection Agency	EPA
Flexural strength	f_r
Flue gas desulfurization material	FGD
Fly ash from Avon Lake PGS	OH
Fly ash from Dolet Hills PGS	DH
Fly ash from Martin Lake PGS	ML
Fly ash from Monticello PGS	MO
Fly ash from Rodemacher PGS	BY
Fly ash	FA
Geopolymer concrete	GPC

Geopolymer paste	GPP
Glass diffraction maximum	GDM
Green house gas	GHG
Least angle shrinkage and selection operator	LASSO
Loss on Ignition	LOI
Mean particle size	$d50$
Million tons	MT
National Center for Environmental Assessment	NCEA
Non-reactive alumina	$NRAl_2O_3$
Non-reactive calcium oxide	$NRCaO$
Non-reactive silica	$NRSiO_2$
Ordinary least squares	OLS
Ordinary Portland cement	OPC
Particle size distribution	PSD
Poisson's ratio	μ
Power generating station	PGS
Reactive alumina	RAl_2O_3
Reactive calcium oxide	$RCaO$
Reactive silica	$RSiO_2$
Scanning electron microscopy	SEM
Specific gravity	SG
Specific surface area	SSA
Thermal resistivity	R

Total alumina equivaltents Al_2O_3

Total calcium oxide equivalents CaO

Total silica equivalets SiO_2

World Business Council for Sustainable Development WBCSD

X-ray diffraction XRD

X-ray fluorescence XRF

ACKNOWLEDGEMENTS

First and foremost, I would like to thank my wife for being by my side through my journey through graduate school. For her continuous support and encouragement, I thank her.

Another person that had a vital role in my studies at Louisiana Tech University was my advisor, Dr. Erez Allouche. I would like to thank him for his guidance, his openness to new and different ideas, his way of disagreeing without disqualifying, his continuous words of encouragement and the freedom he gave me to pursue what I believed in.

I would like to thank Dr. Eklund, Dr. Cardenas, Dr. McKim and Dr. Cahoy for being a part of my advisory committee and providing me with the necessary tools and advice to successfully complete this study.

My sincere gratitude also goes to my friend, Dr. John Matthews, for his always witty advice, and for helping me edit this manuscript. I would also like to thank my friend Eric Stewart for helping me during the mechanical testing and showing me the way in many occasions. I would also like to thank Dr. Carlos Montes for encouraging me to join Louisiana Tech University and for his support, especially at the beginning of my studies.

Finally, my gratitude goes to my friends Shaurav Alam and Dr. Saiprasad Vaidya for their support, advice and encouragement.

CHAPTER 1

INTRODUCTION

1.1. General Introduction

According to the most recent survey released by the American Coal Ash Association (2011), the U.S. produced approximately 135 million tons (MT) of coal combustion products (CCPs) in 2009 making it the second largest by-product stream in the US. The main types of CCPs are fly ash (FA), bottom ash, boiler slag and flue gas desulfurization material (FGD). FA occupies over 45% of the total CCP production with approximately 63 MT per year. FA is composed of fine spherical particles that rise with the flue gases during the combustion of coal which then are captured by pollution control devices. Although 25 of the 63 MT of FA were used beneficially in 2009, 38 MT were disposed in landfills and storage lagoons at a significant cost and posing a potential risk to local aquifers due to possible leaching of heavy metals. However, an imminent change to the current amount of FA used in beneficial applications is expected to happen in the near future. The US Environmental Protection Agency (EPA) is currently developing new regulations with which many of the current beneficial applications of FA, such as soil stabilization and mine reclamation that are considered "un-encapsulated" may be banned allowing only the recycling of FA in encapsulated applications, namely, concrete. In addition, the cost of landfilling operations is expected to increase due to new stricter

1

requirements (liners, groundwater monitoring, etc.) derived from the new regulations (EPA, 2011)

While FA has been used in ordinary concrete as a "supplementary cementitious material" for many years to improve its rheology in the fresh mix and durability of the hardened product, it typically occupies up to 20% of the total mix. However, FA alone is capable of producing a strong cementitious binder when activated under highly alkaline conditions. This binder, often called geopolymer, does not require the presence of ordinary Portland cement (OPC) to harden or gain strength (Davidovits, 1991).

Geopolymers are typically synthesized from materials of geological origin (e.g., metakaolin) or byproducts such as FA that are rich in silica and alumina. Geopolymer binders result from a chemical reaction where silica and alumina molecules contained in an active pozzolanic material (i.e., FA) react under highly alkaline conditions, typically provided by a sodium (or potassium) hydroxide solution and an alkaline silicate (e.g., sodium or potassium silicate). Many researchers agree that the outcome of this reaction is an amorphous 3D network of silicon and aluminum atoms linked by oxygen atoms in a four-fold coordination similar to the one exhibited by zeolites (Fernandez-Jimenez and Palomo, 2004; Davidovits, 1991). The positive ion (Na^+ or K^+) provided by the activator solution serves to balance the negative charge generated by having Al^{3+} atoms in a four-fold coordination. This, gives geopolymer a set of mechanical and chemical properties that are equivalent, or even superior to those of OPC concrete (Provis and van Deventer, 2007; De Silva et al., 2007).

One of the main challenges for a widespread use of FA-based geopolymer concrete (GPC) is the significant variability of FA. Its chemical properties depend on the

type, size and composition of its precursor coal. Silica and alumina molecules contained in the FA are the main components of the geopolymer network thus the amount and ratio of these influence the resulting mechanical properties of geopolymer. However, even though silica and alumina are the main precursors for the geopolymeric reaction, other factors also play a significant role in the mechanical behavior of geopolymer. Impurities, such as CaO, have a positive impact in geopolymer but cause shorter setting times as they create nucleation sites (Temuujin et al., 2009). Another important factor is the fly ash's crystallographic properties (i.e., the way the molecules are arranged within the FA). Since amorphous compounds are easier to dissolve than crystalline compounds during the first step of geopolymerization (dissolution of species), they yield higher amounts of reactive SiO_2 and Al_2O_3 to combine during the transportation/coagulation phase of the geopolymeric reaction, resulting in a higher degree of geopolymerization and consequently higher mechanical strength. The physical properties are mainly a result of the degree of pulverization of the precursor coal, since a significant part of the reaction occurs at the particle-liquid interface, the finer the particles the greater is the surface area and the more reactive is the FA. A second physical factor is the burning efficiency, since a poor burning process yields unburned coal in the FA (quantified as Loss on Ignition, LOI). High content of unburned carbon with high surface area could adversely impact the behavior of the fresh mixture, thereby creating a demand for the addition of activator solution well beyond what is needed to activate the source material, to obtain a workable mixture (Diaz et al., 2010).

This study attempts to provide a series of linear regression models derived from a database of 32 FA stockpiles. Each FA sample was examined in terms of chemical

composition, particle size distribution and crystallographic characteristics. In addition, GPC made from each FA was evaluated in terms of density, setting time, compressive and flexural strength, elastic modulus and Poisson's ratio. The models are an approximation of the true underlying relationship between the aforementioned FA characteristics and the mechanical properties of GPC. It is worth to mention that although the Poisson's ratio was measured for all the samples it was not used in the calculations, since the Poisson's ratio and the elastic modulus are both indicators of the stiffness of the material only one of them was used for the regression modeling; the elastic modulus.

1.2. Research Framework

A significant number of researchers have dedicated efforts to study the chemistry behind geopolymer binders to provide an insight to geopolymerization kinetics. These studies are typically performed using a highly pure source of silica and alumina, such as metakaolin (Provis and van Deventer, 2007; De Silva et al., 2007; Provis et al., 2005). However, FA exhibits a significantly different particle morphology which impacts the mechanical properties of the resulting geopolymer (Provis et al., 2010) and typically contains impurities that fluctuate from one FA source to another, thus they hardly ever extrapolate accurately to FA-based geopolymer. Research efforts have also been made to identify the characteristics inherent to the FA that impact its potential as source material for geopolymerization (Fernandez-Jimenez and Palomo, 2003; van Jaarsveld et al., 2003; Diaz et al. 2010). Although a good approach, it falls short to quantify the tendencies found during the investigations. While the premise "FA with relatively high fineness will produce geopolymer with higher compressive strength" is true and it is indeed useful information, it does not provide specific optimum values or ranges nor takes into account

the interaction of this factor with others that may also affect the mechanical strength of geopolymer.

Other studies have focused on investigations that promote the use of geopolymer highlighting the environmental benefits of recycling FA into geopolymer concrete (van Deventer et al., 2010; Weil et al., 2007). However, these studies fail to solve some of the fundamental issues that prevent GPC from being commercially available in the market.

Also, several researchers have studied the mechanical properties of GPC focusing on the effects that mix proportion, activator solution concentrations, curing conditions, etc. pose on the mechanical properties of GPC (Sofi et al, 2007; Fernandez-Jimenez et al., 2006; Hardjito et al., 2004). To date limited attention was given to evaluating tendencies and correlations within the mechanical properties of GPC for a wide range of FA sources.

A key contribution of the proposed research work is the capturing of the variability posed by using FA stockpiles with a wide range of chemical, crystallographic and physical characteristics as source materials to manufacture geopolymer concrete.

1.3. Objective

The main objective of this research project is to provide an approximation to the true functional relationship between FA characteristics and mechanical properties of GPC through the development of empirical models. These models are aimed at predicting the properties of fresh and hardened GPC using chemical, crystallographic and physical characteristics of FA. In addition, this study attempts to develop linear regression models that capture the mechanical behavior of GPC monoliths.

1.4. Limitations

The present research does not attempt to classify geopolymer with respect to their molecular structures nor attempts to study the kinetics of geopolymerization and chemical reaction products. Instead, it attempts to provide practical forecasting tools that use FA characteristics as input to predict the potential mechanical properties of GPC. Moreover, it attempts to provide empirical equations that explain key relationships that exist within its mechanical attributes.

1.5. Engineering Significance

This study will help to gain better understanding of FA as raw material for GPC by analyzing several FA stockpiles with distinct characteristics and correlating those characteristics with the mechanical properties of GPC. Discerning the relationship between the physical, chemical and crystallographic characteristics of FA and the mechanical properties of GPC is an important step towards producing large quantities of GPC with reasonably consistent and predictive engineering properties.

Another important challenge for the widespread use of GPC is the lack of design equations that represent the correlations and tendencies among its mechanical properties. This study will also attempt to get a better understanding of the mechanical behavior of GPC, based on the effects posed by using different sources of FA. Given that FA stockpiles that possess optimum characteristics will have better geopolymerization potential, thus better mechanical properties compared to others, it is very beneficial to evaluate and compare a statistically meaningful FA database.

CHAPTER 2

LITERATURE REVIEW

2.1. Fly Ash

The combustion of finely ground coal to produce electricity typically leaves behind two main waste streams: (1) bottom ash, composed of particles of sizes ranging from 63 to 1000 μm many times fused together that drop to the bottom of the boiler, hence the term bottom ash; and (2) FA, which is transported along with the flue gases and then captured by pollution control devices namely, electrostatic precipitators or baghouses and occasionally by scrubber systems. Physically, FA is a very fine and powdery material composed mainly of spherically shaped particles that range in size from a few microns to over 100 μm. The chemical composition of FA is very similar to that of volcanic ash having as main components: silica, alumina, iron oxide and calcium oxide in some cases. Typically, a small portion of the chemical components is arranged in a crystalline form (mainly quartz and mullite, but lime, magnetite and traces of others are present in some cases) with the rest being amorphous with no particular arrangement due to its rapid cooling after leaving the boiler (Diaz et al., 2010).

FA is also considered a pozzolan, i.e., a material that will react with calcium hydroxide in the presence of water and create cementitious compounds. Therefore, more than half of the concrete produced in the US uses FA as a partial substitute for OPC in

concrete mixes (Kosmatka et al. 2009). FA is classified, according to ASTM standard C 618, into three different groups:

> Class F. – This type of ash typically results from the burning of anthracite or bituminous coal. However, it can also be produced from burning lignite or subbituminous coal. The sum of its silicon, aluminum and iron oxides must be a minimum of 70% and it must have an LOI of no more than 6%. Its maximum calcium oxide content is set at 10%.

> Class C. – In addition to its pozzolanic properties this type of FA also exhibits some cementitious properties. It is typically derived from lignite and subbituminous coal. However, it can also be the result of burning anthracite and bituminous coal. Its content of silicon, aluminum and iron oxide must add to a minimum of 50% and must have a maximum of 6% LOI. Its calcium oxide content is set to be higher than 10%.

> Class N. – This type of FA groups raw or calcined natural pozzolans such as opaline cherts, shales, volcanic ashes, pumicites and various materials with minimum sum of 70% of silicon, aluminum and iron oxide. It must also have a maximum of 10% LOI among other chemical and physical requirements.

2.2. Cement Footprint

According to a report released in 2009 by the World Business Council for Sustainable Development (WBCSD) the production of OPC is currently responsible for approximately 5% of the total man-made CO_2 emissions in the world, almost equivalent to the amount of CO_2 emitted by all motor vehicles worldwide. OPC is the binder that holds together the second most consumed material (by volume) next to water; ordinary

concrete. The emissions associated with the production of OPC can be divided into two categories: combustion and calcination. Combustion is associated with the fact that the production of cement requires temperatures of approximately 1440°C inside a rotator kiln, consuming significant amounts of energy. Fossil fuels are commonly used to reach such temperatures. The burning of fossil fuels accounts for 40% of the total CO_2 emitted in a cement production process while the remaining 60% is attributed to the calcination process. The calcination of cement's main raw materials to produce clinker releases CO_2, mainly due to the decomposition of $CaCO_3$ into CaO and CO_2. However, it has been suggested that as concrete ages it absorbs back a portion of the CO_2 released during the manufacturing process through its carbonation. It is estimated that, with good recycling practices, 57% of the CO_2 can be reabsorbed through concrete carbonation after 100 years (WBCSD, 2009; Pade and Guimaraes, 2007).

The pollutant nature of cement's production creates an imperative need to develop new construction materials that reduce the human footprint. Furthermore, it presents the opportunity to search for materials that can be recycled to create a strong binder like cement. A great candidate for this is FA. In comparison, the production of one ton of geopolymer binder results in the release of less than 0.2 ton of CO_2.

2.3. Geopolymer

2.3.1. Geopolymer Chemistry

The process through which geopolymers harden is typically referred to as geopolymerization and is carried out by putting FA in contact with an alkaline activator solution, which results in the formation of polymeric chains due to the polycondensation of ortho-sialate ions. While the exact reaction mechanism is not yet understood, it is

commonly assumed that the synthesis is carried out by means of oligomers (a polymer that consist of two, three, or four monomers; e.g., dimmers or trimmers), which provide the unitary structures of the tri-dimensional macromolecular net. Geopolymers based on alumino-silicates are called poly-sialates, or $(-Si-O-Al^-O^-)n$, with the $\underline{n}$ denoting the degree of polymerization. The sialate net consists of SiO_4 and AlO_4 thetahedra linked together by shared oxygen atoms. Inside the cavities of the net, positive ions $(Na^+, K^+, Li^+, Ca^{++}, Ba^{++}, NH_4^+, H_3O^+)$ are present to balance the charge of Al^{3+}, allowing it to be linked to four oxygen atoms. A structural model proposed by Davidovits (1993) is presented in Figure 1. The empirical formula developed by Davidovits (1993) for polysialates can be written as: $Mn(-(SiO_2)_z-AlO_2)n$, where $\underline{M}$ is any of the above mentioned cations, and $\underline{n}$ is the degree of polymerization. The letter z represents 1, 2 or 3, determining the resulting geopolymer net. For the case of z = 1 the net will be of the polysialate type, if z = 2 the net will be a poly(sialate-siloxo), and if z = 3, the net will be a poly(sialate-disiloxo).
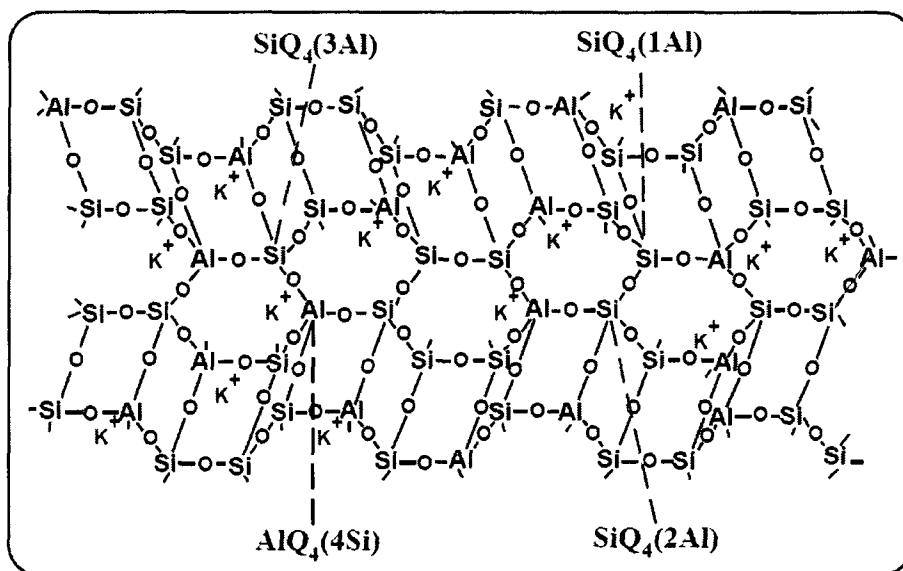
Figure 1 Structural model of geopolymer proposed by J. Davidovits (1993)

Xu and van Denter (2000) proposed that the geopolymerization reaction can be divided into three steps:

1. Dissolution of silicon and aluminum species from the source material through the action of the highly alkaline solution.

2. Transportation of species and formation of monomers (coagulation/gelation).

3. Polycondensation and growth of polymeric structures resulting in the hardening of the material.

However, these steps typically overlap each other under thermal curing and are hard to isolate (Palomo et al., 1999). In addition, some impurities in FA can cause hydration reactions that many times impact the kinetics of geopolymerization. Therefore, since pure geopolymers rarely occur, especially when using FA as source material, many authors refer to geopolymer as Inorganic Polymer Concrete, alkaline cements or Alkaline Activated FA (Fernandez-Jimenez and Palomo, 2004; Sofi et al., 2007). Although some details are still debated, many researchers agree that paralleled to the formation of geopolymer gel, calcium in the mixture reacts with silicate and aluminate monomers dissolved from the source material, forming calcium silicate hydrates (CSH) and calcium aluminosilicate hydrates (CASH). The hydration of these compounds leads to water deficiency and thus raise the alkalinity of the mixture. The increase in alkalinity promotes higher and faster dissolution of silicate and aluminate species from the source material, increasing the rate of poly-condensation/geopolymerization. Thus, the presence of calcium contributes to mechanical strength of the resulting hardened matrix not only by forming CSH and CASH, but also by enhancing the geopolymerization process (Diaz et al., 2010; Temuujin et al., 2009).

2.3.2. Fresh Mix Properties

While OPC is activated with the simple addition of water, FA is activated with a highly alkaline solution in combination with a dense silicate and as a result, GPC fresh mix is typically more viscous than ordinary concrete. Therefore, the use of a water reducer or superplastisizer is recommended to improve the workability of GPC. Figure 2 shows the appearance of a typical GPC fresh mix.

Figure 2 GPC fresh mix

Previous research published by Diaz et al. (2010) proposed that the setting time of geopolymers is highly correlated with the analytical calcium oxide content in FA, stating

that it increases exponentially as the calcium oxide content decreases below 20%. However recent studies have suggested that this relationship may be more complex and require the inclusion of more variables in order to efficiently explain the hardening times of GPC (Chindraprasirt et al., 2011).

2.3.3. Curing

Although some researchers have reported the formation of geopolymer at room temperature (Davidovits, 1999) in order to attain its maximum potential in terms of strength, geopolymer is typically cured under slightly elevated temperature (up to 60°C). Temperature acts as a catalyst accelerating the formation of geopolymer binder and therefore increasing the strength of the resulting concrete. A study performed by Hardjito et al. (2004) showed that the significant maximum compressive strength of GPC can be reached after 48 to 96 hours of curing at 60°C. Conversely, van Jaarsvel et al. (1999) concluded that while mild thermal curing improves the mechanical strength of geopolymer, more aggressive thermal curing (above 70 or 80°C) can be detrimental. This phenomenon is attributed to an excessive loss of water during geopolymerization that compromises the structural integrity causing cracking and shrinkage.

2.3.4. Properties

➢ *Mechanical Properties*

Many studies have reported that GPC possesses mechanical strength that can be similar or even greater than that of ordinary concrete. Sofi et al. (2006) performed a thorough study on the engineering properties of GPC and concluded that its properties are similar to those of ordinary concrete and they have the potential to be predicted by the corresponding Australian Standards. Fernandez-Jimenez et al. (2007) also presented a

study of the mechanical properties of GPC including compressive and flexural strength, modulus of elasticity, bond strength and shrinkage, also with very positive results. The consensus among researchers seems to be that the mechanical behavior of GPC is similar to that of ordinary concrete with flexural strength that correlates to compressive strength in a similar way as it does in OPC-based concretes. Also, the modulus of elasticity and Poisson's ratio values are related to the compressive strength in a similar way as in ordinary concrete.

➢ *Thermal properties*

Geopolymers are particularly resilient in thermal related applications. Research developed by Zuda & Cerny (2009) demonstrated that geopolymers exhibit excellent thermal properties in the range of 20 to 1000°C compared to cement composites at equivalent temperatures. This makes geopolymers exceptionally adequate for applications where high thermal resistivity (R) values are required.

➢ *Corrosion resistance*

The corrosion resistance of geopolymers presents another advantage. As their strength is not based on calcium aluminates that are susceptible to sulfate attack, these materials are practically inert to sulfate induced corrosion. Geopolymer binders are based in an alkaline silicate network, and therefore are inert to the alkali-aggregate reaction which is a relatively common occurrence in ordinary concrete (Allouche et al., 2008). The corrosion resistance capabilities of GPC are illustrated in Figure 3. Here, the results of a test where two geopolymer and two OPC grout samples were submerged in sulfuric acid for eight weeks performed by Allouche et al. (2008) are presented. As seen in the

graph, the GPC samples (especially the class F FA-based geopolymer) performed significantly better than the OPC grout.

REMAINING COMPRESSIVE STRENGTH
after sulfuric acid immersion test (pH = 0.6)
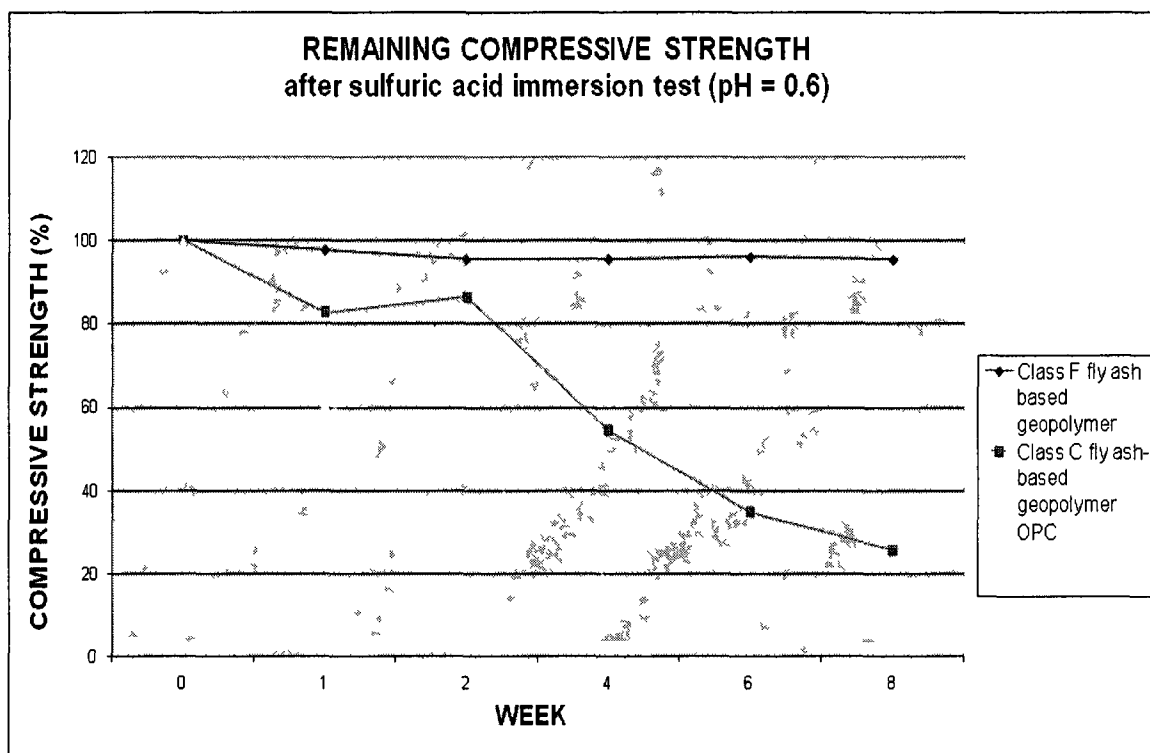
Figure 3 Geopolymer grout corrosion tests performed by Allouche et al. (2008)

2.3.5. Environmental Benefits

One of the main reasons for the growing interest in GPC is its greenhouse gas (GHG) reduction potential The production of Portland cement is responsible for approximately 5% of the total global man-made CO_2 emissions to the atmosphere (WBCSD, 2009). Unlike Portland cement, which requires calcite ($CaCO_3$) as its main raw material, geopolymer could rely on FA. Thus, geopolymers are considered eco-friendly construction materials in two distinct ways: a) reducing the need for Portland cement, and the associated CO_2 emissions; and b) converting CCPs into beneficial construction materials, thus reducing landfill and disposal facility requirements

The development of GPC could contribute to reducing the level of CO_2 emissions with no economic sacrifices, while at the same time converting a potentially hazardous by-product to a valuable construction material. An added benefit is the conservation of landfill space and reduced requirements for storage lagoons, such as the one that failed in Kingston, Tennessee on Dec. 22, 2008 releasing 4.1 million m^3 of FA slurry into the Emory River flooding 12 homes and causing a train wreck (Dewan, 2008).

2.4. Statistical Modeling

Multivariate analysis is a technique often used when studying the effect of more than one variable or regressor in a particular response or set of responses. Amid the multivariate analysis methods, multiple linear regression offers the tools to model the changes of a dependent variable or response when independent variables or regressors fluctuate and the power to predict future responses. The multiple linear regression model is represented by Eq. (1):

$$y = \beta_0 + \beta_1 x_1 + \beta_2 x_2 + \cdots + \beta_k x_k + \varepsilon, \tag{1}$$

where y is the response and ε represents the error of the model. The parameters β_j, $j=0,1,\ldots,k$, are the regression coefficients and x_j are the regressors. The parameter β_j corresponds to the expected change in the response y per unit change in x_j when the rest of the regressors are kept constant. Eq. (1) represents a linear function of the regression parameters, hence the term linear. More information about the fundamentals of multiple linear regression can be found in Montgomery et al. (2006). This method is expected to be a good candidate to analyze the information obtained during this study, discern the complexity of the existing relationships and provide an empirical approximation of the

true underlying mechanisms of FA activation and GPC behavior. However, the coefficients β_j are unknown and have to be estimated.

2.4.1. Ordinary Least Squares (OLS)

OLS is a common technique to estimate the regression coefficients. This technique is based on m inimizing the sum of the square differences between the observations y_i and a straight line i.e. the residual squared error. However, OLS has some drawbacks, as its estimates typically have low bias but large variance, which can result in poor prediction accuracy, and it lacks variable selection capabilities, as in many cases, when there are a large number of regressors often it is desired to keep only the regressors that have the most significant impact in the response and drop the ones that have low impact, which facilitates the interpretation of relationship being modeled (Tibshirani, 1996).

The most noticeable attempts to improve OLS have been the development of subset selection methods and Ridge regression. Subset selection, as the name implies, helps to select the best subsets of a given dataset. However, it is a discrete process where regressors are either retained or dropped from the model depending on their influence. Small changes in the data can produced significantly different models, thus it can be highly variable (Breiman, 1996). On the other hand, in Ridge regression the coefficients are continuously shrunk through a tuning parameter or penalization, thus a more stable process, but variables cannot be set to zero, i.e., all the variables are always kept in the model. For this reason Ridge regression produces models that are hard to interpret (Hoerl and Kennard, 1970).

2.4.2. Least Angle Shrinkage and
Selection Operator (LASSO)

The LASSO method for estimating the regression coefficients in linear regression models was introduced by Tibshirani (1996) to improve the prediction accuracy and interpretation of the OLS technique. It is a penalized least squares method that has the capability to shrink coefficients and set others to zero depending on their effect on the response. Instead of focusing on subsets, LASSO defines a continuous shrinking operation that selects the best predicting subsets and optimizes its coefficients at the same time. Tibshirani (1996) demonstrated that this technique outperforms Ridge regression and subset selection, especially for data with a small to moderate number of moderate-sized effects.

Although the LASSO method has shown success in many situations, it is limited in the following cases: (1) the number of regressors p is greater than the number of observations n. This method can select at most n variables before it saturates; (2) there is a group structure among the predictors with high pairwise correlation. In this case LASSO arbitrarily chooses one variable from the group and drops the rest (3) the regressors are highly correlated. In the presence of multicolinearity the accuracy of the model can be considerably reduced (Zou and Hasti, 2005; Li and Lin, 2010).

2.4.3. Elastic Net

Recently a new regularization technique called Elastic Net (EN) was introduced by Zou and Hasti (2005). EN like LASSO performs variable selection and shrinks the regression coefficients simultaneously through penalized least squares, combining the tuning parameters from Ridge regression and LASSO. I t was demonstrated that EN performs as well as the LASSO whenever this one does its best and overcomes the

limitations that were described above. Simulations and biological data examples were used to show that EN does well in the aforementioned scenarios: (1), (2) and (3). Due to the nature of the data presented in this study, case (3) could be present during the analysis; thus, it should be carefully monitored.

CHAPTER 3

PRELIMINARY EXPERIMENTS

3.1. Overview

This preliminary study was aimed at gaining better understanding of FA as geopolymer precursor by analyzing five FA stockpiles with distinct characteristics and correlating them with the properties of the resulting geopolymers. Identifying which physical, chemical and crystallographic factors of the FA impact the properties GPC is the cornerstone of this study as this allows focusing on variables that truly impact the end product and disregard those have little or no effect.

3.2. Procedures and Equipment

The preliminary study was performed using two class F FA stockpiles and three class C obtained from power plants around the US as potential source material for GPC. Chemical, X-ray diffraction (XRD), scanning electron microscopy (SEM), and particle size distribution (PSD) analyses were performed on the FA samples. Geopolymer paste was analyzed using XRD and Raman spectroscopy. In addition, setting time and compressive strength tests were performed on GPC monoliths.

Four of the five FA samples were collected from lignite-fired power plants located in the Louisiana/Eastern Texas area. The class F FA obtained from Dolet Hills Power Generating Station (PGS) in Mansfield, Louisiana is designated herein as DH; the

class C FA from Monticello PGS in Mount Pleasant, Texas as MO; the class C FA from Martin Lake PGS in Tatum, Texas as ML, and the class C recovered from Rodemacher PGS in Boyce, Louisiana, is referred to as BY. An additional class F FA sample (OH) was collected from a bituminous coal-burning PGS in Avon Lake, Ohio.

Chemical analysis of the FA stockpiles was performed via X-ray Fluorescence (XRF) following ASTM standard D-4326. PSD analysis was conducted using a Microtrac S3500 laser-based equipment with a measuring range between 0.024 μm and 2816 μm. Samples were suspended in Isopropyl alcohol and went through the necessary cycles of reading and dispersing using ultrasound, to obtain a realistic analysis.

XRD data was obtained using a Bragg-Brentano geometry powder diffractometer using a copper anode at 40 kV. Data was collected between 10° and 65° of two theta angles, with a step size of 0.05° and a count time of 5 s per step. Samples were further analyzed using the Rietveld phase quantification method to determine the amount of crystalline and amorphous components.

SEM micrographs of untreated and treated samples were taken using Hitachi S-4800 scanning electron microscope. SEM was performed to show the ash particles before and after the geopolymerization process.

Geopolymer paste samples were also analyzed using Raman spectroscopy. Spectra from 200 to 2700 cm^{-1} were collected on an R-3000-HR Raman spectrometer from Raman Systems using a 785 nm diode laser operating at 290 mW through a fiber optic probe.

The mix design for the concrete specimens is presented in Table 1. It was established using the absolute volume method proposed by the Portland Cement

Association (Kosmatka et al., 2009). It is worth mentioning that the quantities provided in Table 1 are estimates since there were small variations as the activator solution to FA ratio was adjusted depending on the liquid demand of each FA stockpile to obtain a slump of 10 to 15 cm, i.e., the amount of FA, sand and gravel in the mixture varied slightly as more or less activator solution was added to obtain the desired slump value. The activator solution used was composed of a 14 M NaOH solution and Sodium Silicate type "D" from PQ Corporation (45% by weight and SiO_2 to Na_2O ratio of 2:1). Tap water was used throughout the experiments in an attempt to mimic field conditions. The two solutions were mixed in a 1:1 ratio by weight. Well graded sand with a bulk density of 1680 kg/m^3 (100 lb/ft^3), a specific gravity of 2.63 and a fineness modulus of 2.4 served as fine aggregate. "Pea gravel" (1 cm or 3/8 in. diameter) with a bulk density of 1934 kg/m^3 (115 lb/ft^3) and specific gravity of 2.70 acted as coarse aggregate. In order to improve the workability of fresh GPC, the superplastisizer Glenium 7101® (manufactured by BASF) was incorporated 60 s before the end of the mixing cycle. The ingredients were mixed in a vertical mixer with planetary action (beater rotates in its axis in opposite directions as it moves around the bowl). In order to promote the first phase of geopolymerization, dissolution of silicate and aluminate species, the following mixing procedure was utilized: (1) FA and NaOH solution were mixed for 30 s; (2) sodium silicate was added and mixed for 30 s; (3) sand was added and mixed for 60 s; and finally, (4) gravel was added and mixed for an extra 120 s (Glenium was added 60 s before the end of the mixing cycle). Due to BY's short setting time, mixing times were shortened enough to cast and form the specimens. The samples were poured into 75x150 mm cylinders and their compressive strength was determined following ASTM standard C-39. Setting time

measurements of fresh geopolymer paste were taken using a standard Vicat needle. All samples were stripped from the mold after 24 hrs, cured for three days at 60°C, taken out of the oven and let to cool down at room temperature for 24 hrs prior to testing.

Table 1 Mix proportions for the concrete samples*

Material	Quantity (kg/m^3)
Fly Ash	494
Sand	691
Gravel	858
Activator Solution	198-464
Superplastisizer	15

* Values will vary depending on the activator solution demand

3.3. Results of Preliminary Study

3.3.1. Fly Ash Chemical Composition

The chemical composition of the FA samples is summarized in Table 2. It is important to mention that the values reported in Table 2 are equivalents in their respective oxide form, as these may be combined in more complex crystalline or amorphous phases. The chemical composition is given in equivalents throughout this manuscript, this helps to simplify the analysis and have a better perspective of the chemical composition.

Table 2 Preliminary XRF results

	BY (%)	MO (%)	DH (%)	ML (%)	OH (%)
Type	C	C	F	C	F
SiO_2	37.77	55.61	58.52	48.7	55.07
Al_2O_3	19.13	19.87	20.61	16.6	28.61
SiO_2/Al_2O_3	1.97	2.8	2.84	2.93	1.92
$SiO_2+Al_2O_3$	56.9	75.48	79.13	65.3	83.68
CaO	22.45	12.93	5	18.72	1.97
Fe_2O_3	7.33	4.52	9.43	6.93	6.22
MgO	4.81	2.49	1.86	3.91	1.08
SO_3	1.56	0.49	0.49	0.85	0.19
Na_2O	1.8	0.67	0.52	-	0.38
K_2O	-	0.86	-	-	2.63
Mc[a]	0.12	0.02	0.14	0.12	0.12
LOI[b]	0.17	0.22	0.05	0.49	1.82
Total	93.05	95.91	96.43	95.71	96.15

[a]Mc=Moisture Content
[b]LOI=Loss on Ignition

The SiO_2/Al_2O_3 ratio ranges between 1.92 and 2.93 and the silica plus alumina content ranges from 56.90% and 83.68%, with BY having the lowest concentration and OH the highest. These are the basic ingredients of the geopolymeric reaction and they are within the range of values reported by others (Davidovits, 199; Palomo et al., 1999). CaO, in the case of BY, MO and ML, is the third most abundant oxide in the FA samples ranging from 12.93% to 22.45%. Smaller amounts were found for OH and DH (1.97% and 5.00%, respectively). Calcium content has been reported to have significant influence on the properties of the fresh mixture as well as the properties of the final hardened product (Temuujin et al., 2009). Fe_2O_3 is the fourth most important compound ranging from 4.52%, in the case of MO, to 9.43% in the case of DH. LOI for the BY, MO, DH and ML samples was below 0.50%, while a value of 1.82% was found in the case of OH.

LOI is a critical factor when assessing the geopolymerization potential for a given FA. Unburned carbon absorbs the activator solution, and thus obtaining a workable mixture requires a volume of activator solution well beyond that needed to merely activate the source material. This results in lower mechanical strength and higher costs.

3.3.2. Fly Ash PSD

PSD curves showing cumulative values for the five FA samples are presented in Figure 4. The BY sample had the greatest percentage of particles passing 45 μm followed by DH, OH, ML and MO. ML and BY FA samples were found to contain a significant amount of particles below 1 μm (around 34%). OH, MO and DH were found to have lower fraction of extra fine particles, however, this was compensated by a larger fraction of particles ranging from 4 to 20 μm. PSD is among the most important physical properties impacting the reactivity of FA and the resulting geopolymer product (van Jaarsveld et al., 2003). Because a significant part of the reaction occurs at the particle-liquid interface, the finer the particles, the greater the surface area and the more reactive is the FA.
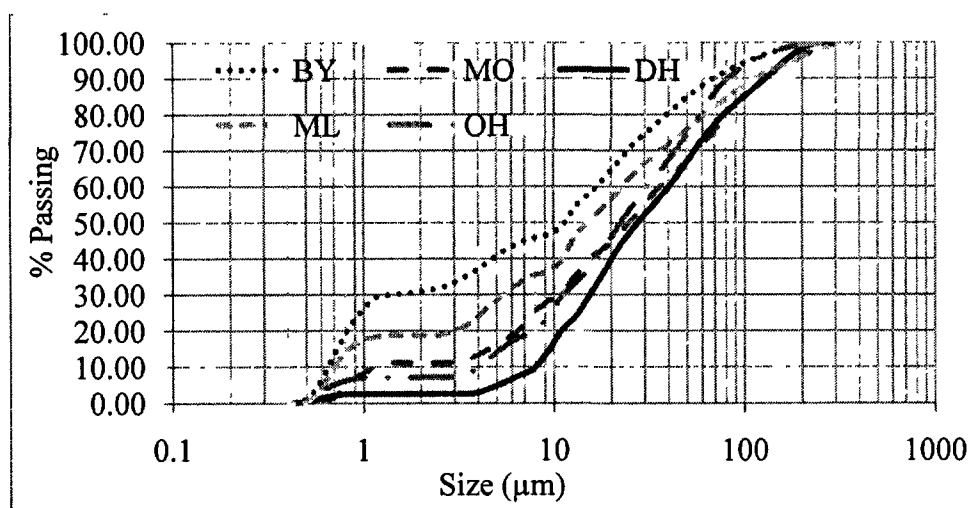
Figure 4 Particle size distribution curves

3.3.3. SEM Analysis

Figure 5 shows SEM micrographs of FA before geopolymerization (left) and after (right). The morphology of FA particles is predominantly spherical. The role of particle morphology has been emphasized by many authors for its significant impact on the resulting geopolymer (Provis et al., 2010; Hunger and Brouwers, 2009). The image showing FA after the activation process clearly shows the formation of geopolymer gel and also suggests that larger particles (>20 μm) do not react chemically, but become physically embedded in the reacted binder.
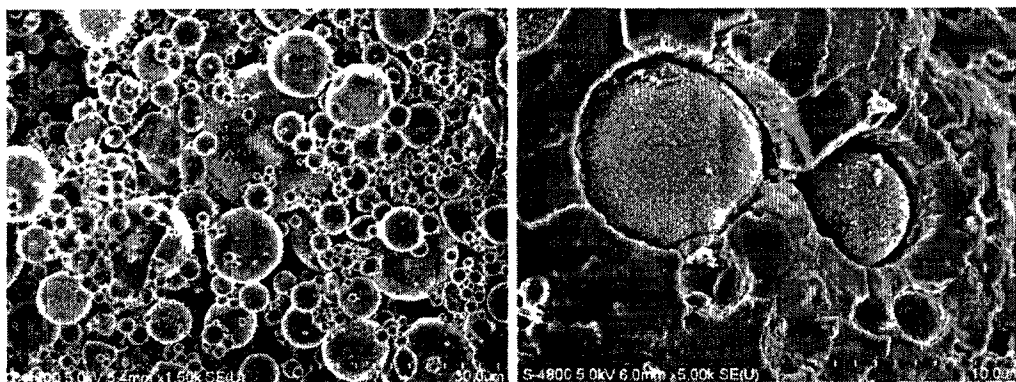
Figure 5 SEM micrographs of FA before geopolymerization (left) and after (right)

3.3.4. XRD Analysis

Figure 6 shows XRD patterns for FA and hardened geopolymer paste (GPP). The samples are mostly composed by a vitreous phase. Quartz is found in small amounts and in some cases mullite, merwinite, calcite and traces of other crystalline phases are found as well. The patterns also show that crystalline phases still remain after the geopolymerization, although in smaller amounts. An important crystallographic factor to consider when working with relatively high calcium FA is the location of the glass diffraction maximum (GDM), a broad elevation in the X-ray pattern forming a bump instead of a normal sharp peak. Previous studies have shown that the location of the GDM in FA stockpiles containing up to about 20% analytical CaO is typical of a siliceous glass structure (2θ values of $22.7°$ to $27.5°$). For FA stockpiles with analytical CaO contents above 20% the location of the GDM remains around $32°$ 2θ, a value typical of calcium aluminate glass structure that is significantly more reactive with water compared with the siliceous glass structure (Diamond, 1983). This leads to the formation of calcium silicate hydrate compounds additional to the geopolymerization products, augmenting the mechanical strength of the hardened matrix.
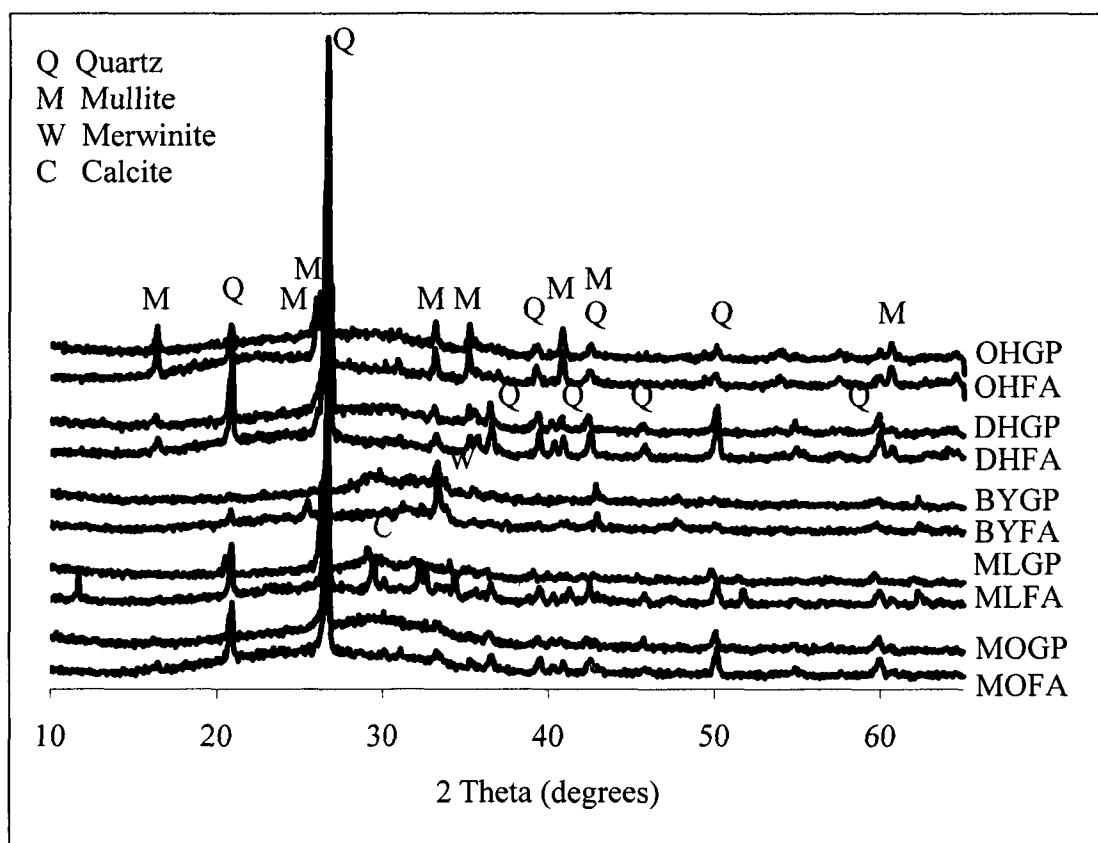
Figure 6 XRD patterns for FA and hardened geopolymer paste (GPP)

3.3.5. Raman Spectroscopy
Analysis

Raman patterns for GPP are shown in Figure 7. Broad Raman shifts can be detected peaking around 355 cm^{-1} for GPPs prepared using BY, ML, DH and MO FA stockpiles. For GPPs made with BY and ML ashes an additional shift can be detected at 1000 cm^{-1}. OH shows no Raman shifts at 355 cm^{-1} on the analysis. The formation of calcium hydroxide can be monitored using Raman spectroscopy due to hydroxide vibration observed around 355 cm^{-1} (Potgieter-Vermaak, 2006, Diaz et al., 2010). Raman Spectroscopy was introduced to this research as a useful method for detecting Calcium activity in geopolymer paste samples and as a mean of corroborating the calcium content reported by the chemical and XRD analyses.
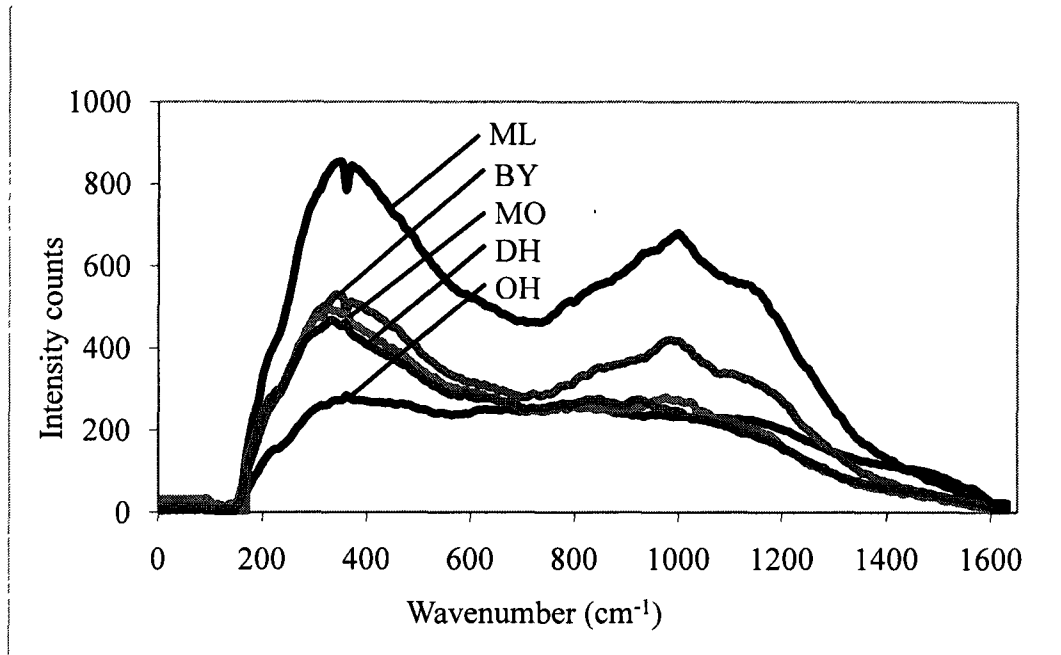
Figure 7 Raman spectroscopy patterns for hardened geopolymer paste

3.3.6. Setting Time and Compressive Strength

Table 3 summarizes the mechanical properties of the resulting geopolymer concretes. BY had the shortest setting time with only 1.5 min., followed by ML with 17 min. and MO with 25 min. DH set after 3 hrs and OH did not set after 5 hrs at room temperature, thus a slight increase in temperature was required to kick start the geopolymerization reaction. The compressive strength tests also revealed a wide range of performance from 40 MPa (DH) to 80 MPa (ML). It is worth noting that typical construction applications require a 28-day compressive strength of 25 MPa to 40 MPa.

Table 3 Summary of results and factors that influence the compressive strength

	ML	BY	MO	OH	DH
Compressive strength (MPa)	80	60	56	47	40
Setting time (min)	17	1.5	25	300	180
CaO	2	1	3	5	4
Total glass	2	4	1	3	5
Particles passing 45μ	4	1	5	3	2
Total	8	6	9	11	11

1= Highest content relative to the rest of the fly ashes
5= Lowest content relative to the rest of the fly ashes

3.4. Summary of Preliminary Testing

Although there are several mix design parameters that can be modified to increase or decrease the mechanical strength of geopolymer such as $NaOH/Na_2SiO_3$ ratio and activator solution to FA ratio, there are many others that are inherent to the FA precursor that dictate the behavior of the fresh mixture and the resultant mechanical properties of the hardened matrix. The main three are the chemical, crystallographic and physical properties of the FA.

Although silica and alumina are the main precursors for the geopolymeric reaction, other factors seem to also play a significant role in the resultant compressive strength. For example, OH has the greatest amount of silica + alumina (83.68%), however, it yielded the second lowest compressive strength. BY and ML have the lowest silica + alumina contents, but exhibited the highest compressive strengths. This can be attributed to the high CaO content and high percentage of fine particles below 5 μm. The calcium activity is corroborated by the RAMAN Spectroscopy analysis. An examination of Figure 7 reveals that BY, ML, MO and DH show a broad peak at 355 cm^{-1},

characteristic of calcium hydroxide activity, whereas OH showed little disturbance in the spectrum, which correlates well with low calcium content.

The location of the GDM for different FA stockpiles is shown in Figure 8. For OH, DH, ML, and MO FA sources, the GDM is characteristic of a siliceous glass structure, although allowing some calcium silicate glass in the system. Despite migration of the GDM to the right as calcium content increases, the structure remains primarily siliceous glass. Conversely, the BY stockpile shows a GDM indicative of a dominant calcium silicate glass structure, which is more reactive with water and tend to form calcium silicate hydrated compounds that boost the mechanical strength values of the resultant geopolymer. Although the analytical CaO content does not represent all of the CaO in the glass phase (a small amount of calcium is contained in the crystalline phases), there is a strong correlation between the analytical CaO content and the location of the GDM. Figure 9 shows this correlation, and to support its validity for other FA sources data reported by Diamond S. (1983) from 16 FA stockpiles was also included.
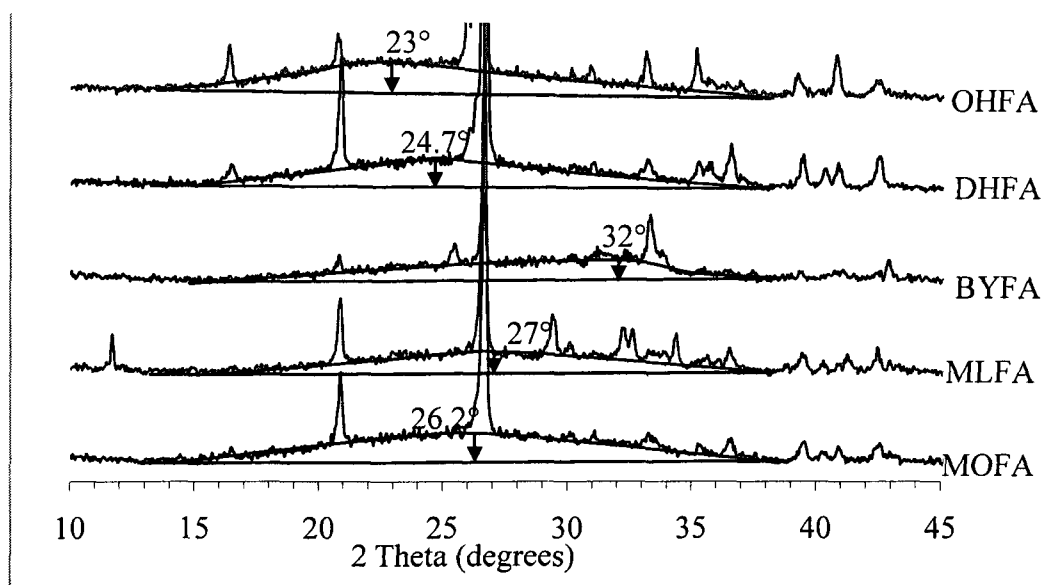
Figure 8 Location of the GDM
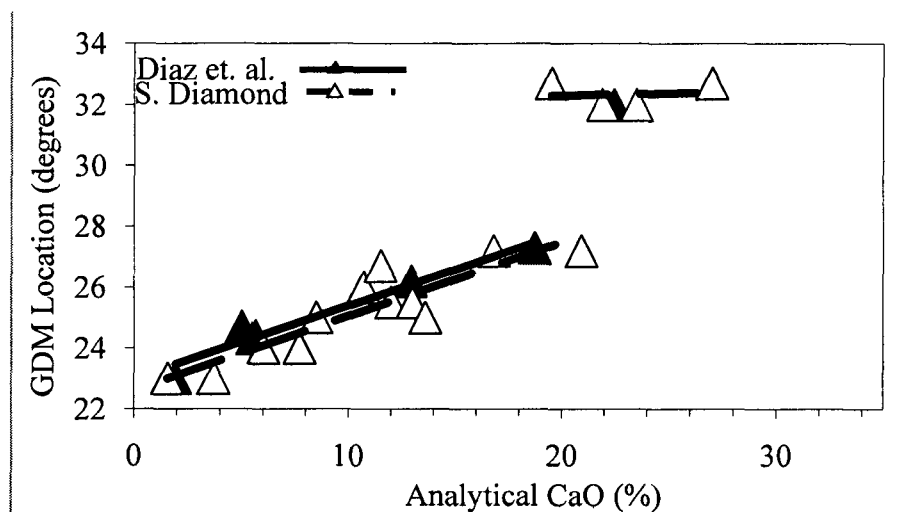
Figure 9 Correlation between analytical CaO% and the location of the GDM

The setting time of GPC seems to be governed by the type of glass structure prevailing in the FA. Given the higher reactivity of calcium silicate glass with water compared to siliceous glass, it is expected that as the fraction of calcium silicate glass increases the setting time decreases, and at the same time the compressive strength increases. This correlation, presented in terms of analytical CaO content versus setting time and compressive strength is shown in Figure 10.
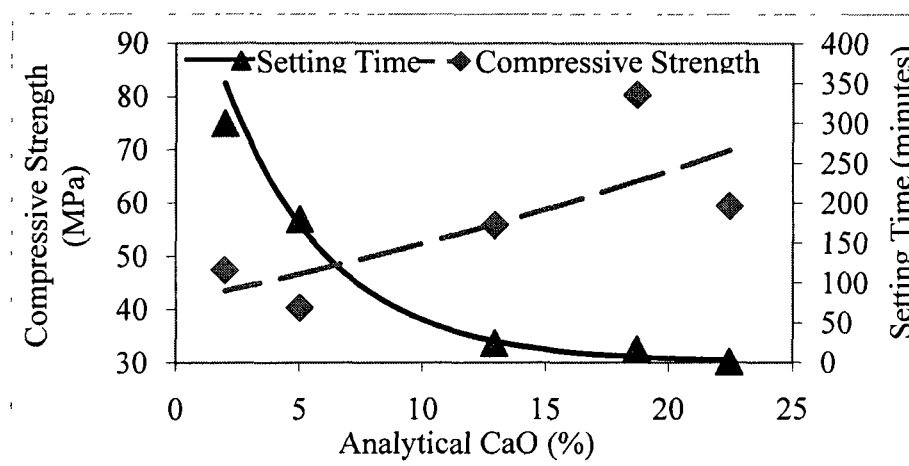
Figure 10 Correlation between analytical CaO%, compressive strength and setting time of geopolymer concrete

Although increasing CaO content in FA seems to have a positive influence on the compressive strength of the resulting geopolymer, FA stockpiles with analytical CaO content higher than 20% will exhibit very rapid setting (less than 3 min.), thus they are not recommended as source material for geopolymer.

The total amount of glass phase is closely related to the cooling rate of FA after the combustion process. Slow cooling rates will allow higher degree of crystal formation, resulting in less glass phase and vice versa. The total glass phase in the FA is also a factor affecting geopolymerization since glass phase is easier to dissolve by the alkaline activator, therefore releasing more geopolymer precursor species into the system. Figure 11 shows the distribution of glass and crystalline phases in the FA and the resultant geopolymer. It can be seen that in all cases the amount of glass phase is higher in the geopolymer than in its FA precursor, however, the change in glass phase between the FA precursor and the resultant geopolymer paste varies significantly among the different stockpiles. This could be attributed to the fraction of crystalline phases dissolved during the activation process and transformed to amorphous geopolymer.
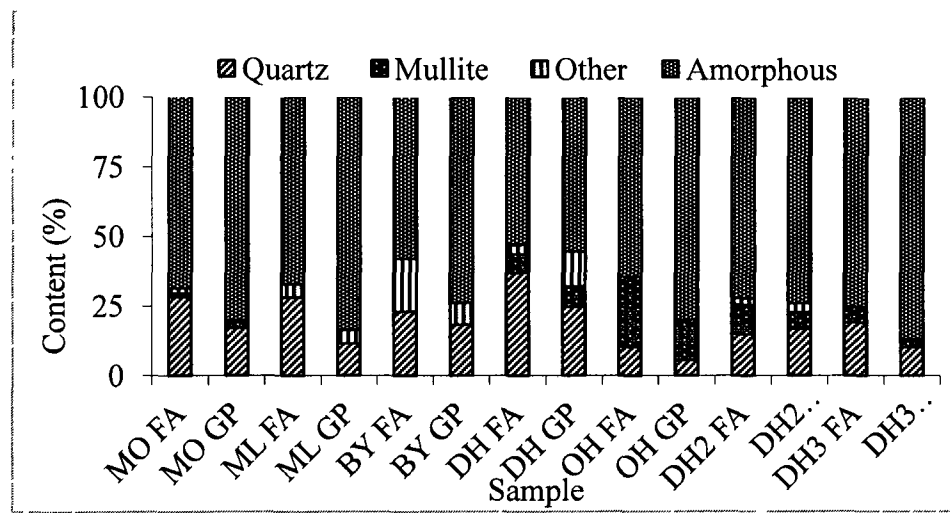
Figure 11 Total glass phase for fly ash stockpiles and hardened geopolymer paste

The relatively high LOI (indicating mainly unburned coal) of OH stockpile resulted in a more hygroscopic mixture, thus additional activator solution was needed to obtain the desired consistency. The lower compressive strength of the OH geopolymer could be attributed to this factor.

Table 3 presents a summary of the factors inherent to the FA, that affect the mechanical strength of the resultant geopolymer. Values one to five were assigned to the FA stockpiles for each factor, i.e., one indicates the highest rank with respect to the value of a particular factor (e.g. CaO content) compared with those of the fly ashes and five the lowest. The ranks of each FA precursor for these three categories were summed to give an overall score. It can be seen that a correlation exists between the FA precursor CaO content, PSD and percentage of total glass phase and the compressive strength of the resulting geopolymer.

3.5. Lessons Learned from Preliminary Tests

Factors inherent to the FA stockpiles tested during this investigation that have more pronounced effects on the mechanical strength of the hardened paste and behavior of the fresh mixture are the location of the GDM (which is related to the analytical CaO content), the total glass phase content in the FA and the particle size distribution. The setting time increases exponentially as the CaO content decreases below 20%, however the decrease in CaO was accompanied by a decline in the compressive strength of the resulting geopolymer. Based on the FA stockpiles tested in this work a CaO content range of 5% to 15% might be considered desirable for many applications. Additionally, this overrules the threshold of 10% analytical CaO set by ASTM C 618 for class C and F

FA for use in concrete. For geopolymer manufacturing there is a clear threshold at 20% of analytical CaO related to the dominant amorphous phase and setting time.

The degree of vitrification during the cooling of FA plays an important role in geopolymerization. FA with high content of glass phase will lead to higher degree of geopolymerization, therefore, higher compressive strength. This parameter can be controlled at the power plant, increasing the suitability of the FA to geopolymerization. Particle size distribution has a significant impact in the reactivity of FA. Higher amount of fine particles will result in higher surface area, and therefore higher reactivity, resulting in higher compressive strength. Thus, grinding of FA might be under-taken to enhance its suitability to geopolymerization.

The presence of unburned coal in FA, even in relatively small amounts, will require higher activator solution to FA ratio, which results in an adverse effect on the compressive strength of the hardened geopolymer paste as well as economic disadvantage in the manufacturing of the geopolymer concrete (i.e., activator solution represents a major cost item in the production of geopolymer concrete).

CHAPTER 4

MATERIALS AND METHODS

4.1. Materials

This study was based on the analysis of 32 FA samples (including the ones from the preliminary experiments) collected from power generating stations around the US. The database of FA samples was partitioned into two individual sets: the first consisting of 24 samples for data analysis and model building, and the second consisting of the eight remaining samples for validation purposes. The first set has 14 samples that are classified as type F and 10 as type C according to ASTM specification C 618. The second set has five type F and three type C.

The testing was performed under the same conditions and using the same sand, gravel, sodium silicate, sodium hydroxide and superplastisizer with the same concentration, and in the same ratio of materials as in the preliminary experiments. For a full description of these, please refer to Chapter 3.

4.2. Methods

4.2.1. Characterization of FA, GPP and GPC

The 32 samples were analyzed via XRF and XRD to obtain their chemical and crystallographic composition. PSD was also obtained to monitor the physical characteristics. In addition, hardened geopolymer paste was also analyzed via XRD.

According to the preliminary experiments, these characterization methods would be the most significant to create a regression model. The XRD, XRF and PSD were performed in the same manner, using the same equipment and following the same ASTM standards as stated in Section 3 2. The mix design from the preliminary tests (shown in Table 1) was adopted for the rest of the study with the same provision, i.e., the quantities stipulated in Table 1 are estimates given that the activator solution to FA ratio will vary depending on the FA. The same planetary mixer and mixing sequence used in the preliminary experiments was used throughout the rest of the study.

The fresh mixture was cast into 15x30 cm cylindrical molds to be tested as per ASTM standard C 39 for compressive strength and ASTM C 469 for static elastic modulus and Poisson's ratio (Figure 12).

Figure 12 Testing static elastic modulus of GPC

GPC mixture was also cast into 10x10x40 cm rectangular prism molds for flexural strength testing (third-point loading) as per ASTM standard C 78 (Figure 13). Concrete density measurements were taken following ASTM C 138. Setting time measurements were taken on geopolymer paste using a standard Vicat needle. Each data point presented in this study is an average of three measurements with less than 8% variation or two measurements with less than 6% variation. All samples were stripped from the mold after 24 hrs, cured at 60°C for 72 hrs, and then cooled down for 24 hrs prior to testing. It is worth noting that the significant maximum (90 to 95%) cylinder compressive strength and flexural strength of GPC is commonly achieved within three to five days depending on the curing effort applied (Hardjito et al., 2004).
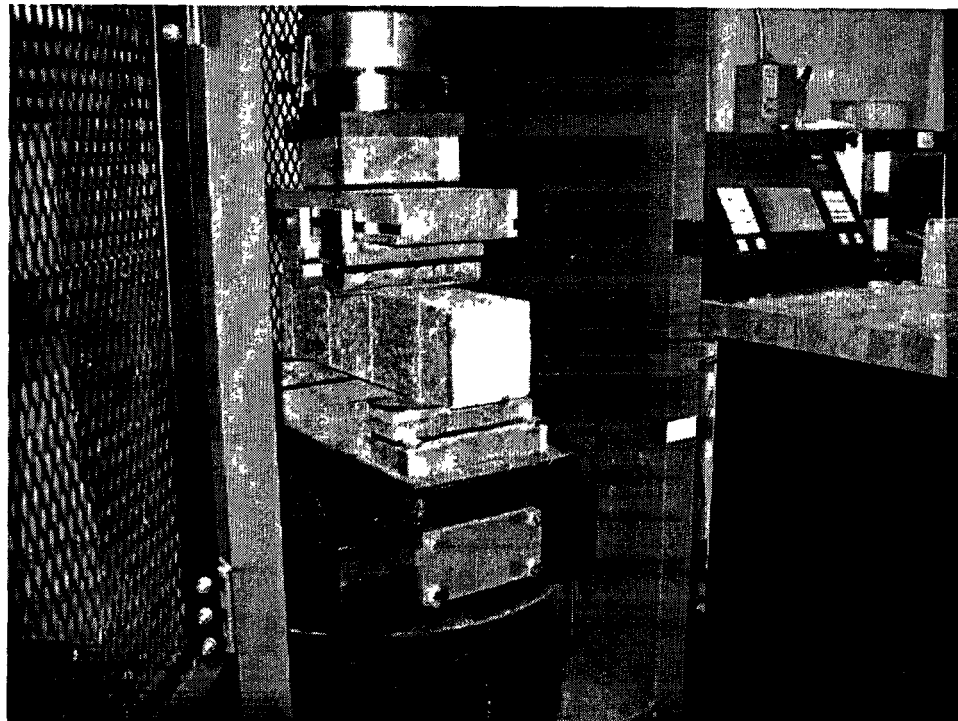
Figure 13 Testing flexural strength of GPC

4.2.2. Statistical Tools

> *R software*

R is a computer software and language designed for statistical computing and graphing. It was developed in Bell Laboratories (formerly AT&T, now Lucent Technologies). R offers a wide range of capabilities, including multiple regression analysis, non-linear modeling, clustering and many more. It is also able to generate publication-quality graphs and although R is an open source program, it is well established and accepted by the scientific community. One example of the use of this software is to support toxicity assessment for acute inhalation exposure by the EPA's National Center for Environmental Assessment (NCEA). A screenshot of "R" is shown in Figure 14.
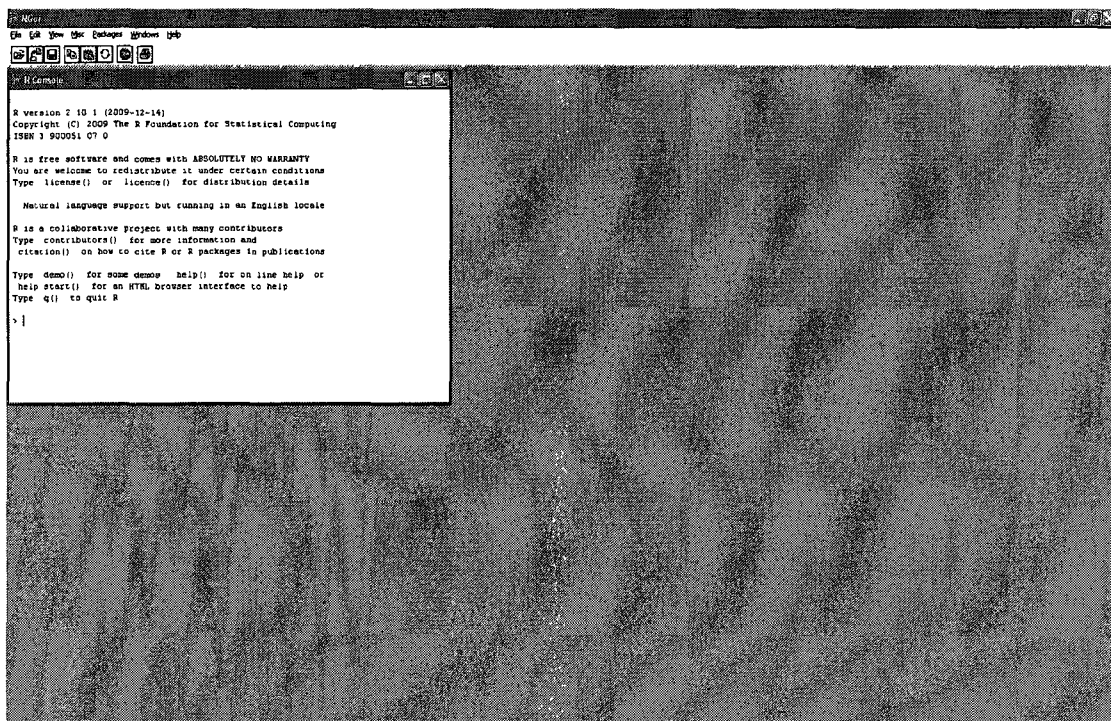
Figure 14 Screenshot of software "R"

> *LEAPS package*

LEAPS is a package contained in R for subset selection in multiple linear regression. It performs an exhaustive search of the best subsets of regressors for predicting a particular response. It uses a branch and bound algorithm and OLS to select the most influential regressors and the optimum number of these to predict a response. The output is the best combination of predictors at all the possible degrees of freedom for predicting the response, i.e., the outcome includes the best predictor for a model with only one variable, the best predictors for a two variable model, and so on until all the possible predictors are included in the model. Adjusted R^2 or Mallow's Cp values are available in the output to assess the fit of the subsets (Lumley, 2009).

> *LARS package*

LARS was released in 2007 as a tool to perform LASSO, least angle and forward stagewise regression. It provides efficient procedures to fit an entire LASSO sequence by shrinking coefficients, and selecting variables simultaneously, and it has the capability to compute the k-fold cross-validated mean squared error, plot and predict new observations. The output includes plots, entire paths of solutions or solutions at a particular point along the path for coefficients and fitted values and an analysis of variance-type summary. The Mallow's Cp values, residual sum of squares and the degrees of freedom are also available to assess the models (Hasti and Efron, 2007).

> *GLMNET package*

This package was incorporated into the R database in early 2011 as an efficient tool to select and estimate regression coefficients using the EN algorithm. GLMNET provides the necessary procedures to fit an entire EN regularization path for linear

regression using cyclical coordinate descent in a pathwise fashion. Similar to LARS, it has the capability to compute a k-fold cross-validation, plot and predict new observations either throughout entire paths of solutions or at a particular point. The output includes the optimum parameters to fit a regression model with the EN algorithm.

CHAPTER 5

RESULTS

5.1. Fly Ash

5.1.1. Chemical Composition

Table A.1 shows the chemical composition of the FA samples used in the statistical analysis. Silica and alumina are the basic ingredients of the geopolymeric reaction and they were found to be within the range of values reported by others (Davidovits, 1999; Palomo et al., 1999). Calcium oxide is also present in all FA samples at different extents and should be carefully monitored during the analysis given that is one of the impurities in FA that has a significant impact on the characteristics of the resulting geopolymer due to its tendency to form hydration products and modify the conditions of the geopolymerization reaction (Temuujin et al., 2009). LOI was found in the majority of the samples. Its presence is believed to have a significant influence on the hygroscopic characteristics of the FA, as the highly porous unburned coal tends to absorb the activator solution, and thus the mixture requires a volume of solution well beyond that needed to merely activate the FA (Diaz et al., 2010).

5.1.2. Crystallographic Analysis

Table A.2. shows a list of the crystalline phases found in the samples with a letter or set of letters assigned to each phase to facilitate calculations presented later in this report. The results of the XRD quantitative analysis for each FA stoc kpile and the

42

resulting GPP are presented in Tables A.3. through A.9. All samples are predominantly amorphous, containing relatively small amounts of quartz and nearly all samples contain mullite. Traces of other crystalline phases can also be found. Amorphous compounds are easier to dissolve than crystalline compounds during the first step of geopolymerization (dissolution of species), yielding higher amounts of reactive SiO_2 and Al_2O_3 to combine during the transportation/coagulation phase of the geopolymeric reaction, therefore resulting in a higher degree of geopolymerization and consequently higher mechanical strength (Fernandez-Jimenez and Palomo, 2003; van Jaarsveld et al., 2003).

5.1.3. Particle Size Distribution and Specific Surface Area

The particle size distribution curves of selected samples are shown in Figure 15. Also, a summary of the physical properties of the FA samples including specific surface area and mean particle size is given in Table A.9. PSD is among the most important physical properties impacting the reactivity of FA and the resulting geopolymer product (Palomo et al., 1999). Geopolymeric reaction, like hydration in cement, occurs mostly at the surface of the particles; smaller particles will result in greater surface area, and therefore higher reactivity in the FA. Researchers (Hunger et al., 2009; Martin et al., 2009) have highlighted the importance of powder PSD with respect to their application in concrete. The powder in a concrete mix provides by far the highest percentage of surface area with respect to the other solids (sand and gravel) in the mix. Therefore, its packing characteristics have a significant impact in the workability of fresh concrete and the water it demands. In many occasions, it also dominates the physical properties of the hardened product such as strength and durability.
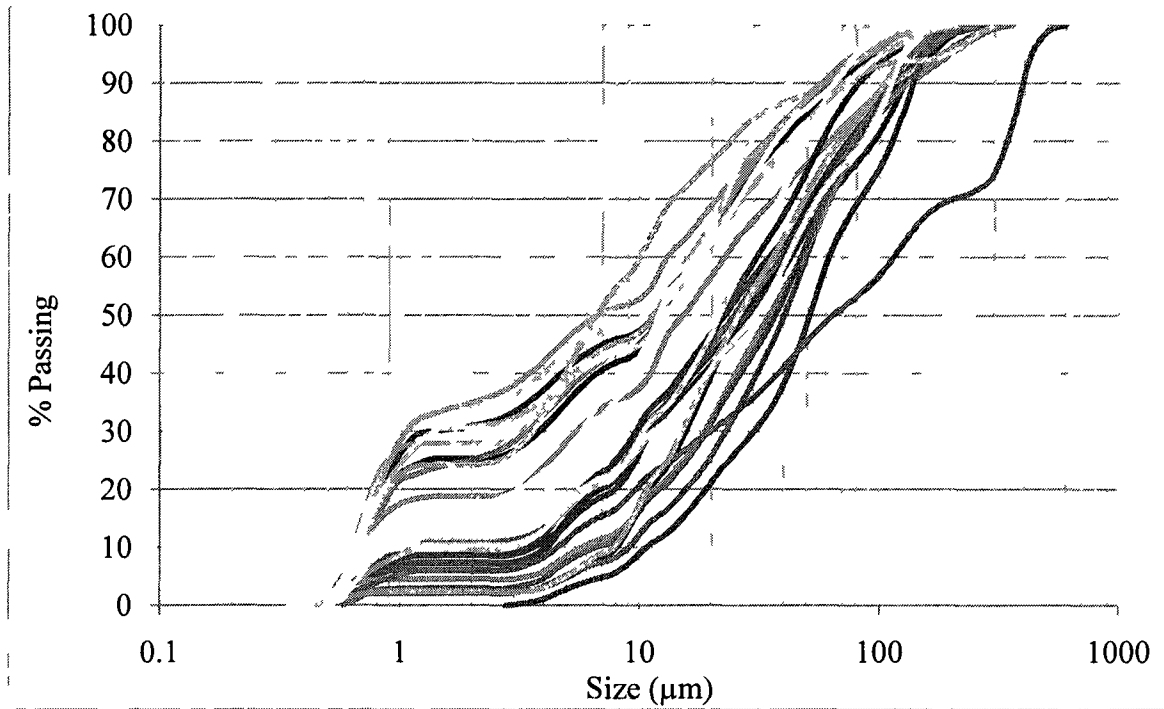
Figure 15 Particle size distribution curves of selected FA samples

5.2. Fresh Mix and Mechanical Properties of GPC

A summary of the fresh mix and mechanical properties measured for each of the GPC samples is presented in Table A.10. Density values ranged from 1,890 to 2,371 kg/m³. The cylinder compressive strength ranged from 5.53 to 64.68 MPa, while the flexural strength ranged from 1.15 to 6.31 MPa. The flexural strength was between 8% and 26% of the compressive strength, compared to a range of 9 to 12% typically cited for OPC concrete (Macgregor and Wight, 2005). The static elastic modulus varied from 4,619 to 42,878 MPa. Separate values for the class C and class F FA-based GPC are also given in Table A.11. Poisson's ratio exhibited values ranging from 0.08 to 0.22. These appear to reside towards the low end of the range typically cited for OPC concrete (0.15 to 0.22) (Macgregor and Wight, 2005). Setting time values ranged from 2 to 480 min. Images showing the mechanical testing can be found in Figure C.1 of Appendix C.

CHAPTER 6

ANALYSIS OF RESULTS AND DISCUSSION

6.1. Evaluating the Impact of FA Characteristics in the Resulting GPC

The attributes of GPC that are considerably influenced by FA characteristics are the density of the fresh mix, the setting time and the overall mechanical properties. As expected, the density of the fresh mix is influenced mainly by the physical characteristics of FA, i.e., specific gravity, particle size, etc. This can be attributed to the varying interstice systems that can be present in the FA samples. The setting time is influenced mainly by the CaO content in FA as proposed in the preliminary study. In the case of the mechanical properties, in order to reduce the number of dependant variables, only the compressive strength values were used as response to perform the evaluation. However, the flexural strength and elastic modulus can be obtained using the compressive strength as shown in later sections. The compressive strength of GPC is dependent on a complex fusion of physical, chemical and crystallographic factors of FA.

6.1.1. Preparing the Data for Statistical Analysis

Although silica and alumina are the main precursors for the formation of the geopolymer network and calcium oxide has significant influence in the chemical structure of the binder, these values cannot be taken from the XRF analysis without taking into consideration their crystalline arrangement since they represent absolute totals

45

regardless of their reactivity. The preliminary studies showed that the crystalline part of FA stays nearly inert while the amorphous component is the reactive one throughout the geopolymerization reaction. Therefore, the amount of silica, alumina and calcium oxide in a crystalline arrangement was not taken into account in the analysis and it was assumed that only the amorphous components participate in the geopolymerization reaction. In addition, given that the total silica, alumina, lime and LOI are calculated as percentages of the same analysis, potential multicolinearity problems could be avoided by incorporating the crystalline distribution results to the chemical analysis.

Each crystalline phase is composed of one or more elements in the form of oxides, e.g., Mullite is composed of 71.79% Al_2O_3 and 28.21% SiO_2. The chemical composition of each crystalline phase containing silica, alumina and calcium oxide in the FA samples is shown in Table A.12. Using these values, the crystalline components obtained by XRD were be subtracted from the total values obtained by XRF. To illustrate this process, sample one is used as an example:

Step 1. – Crystalline phases in the FA sample containing silica, alumina or calcium oxide are identified using Tables A.3 through A.9. For sample 1, these are phases Lime, Merwinite and Quartz (R, U and AF as categorized in Table A.2.).

Step 2. – The chemical composition of the crystalline phases is identified (from Table A.11). AF contains 100% SiO_2. U contains 36.56% SiO_2, 51.18% CaO and 12.26% MgO. R contains 100% CaO.

Step 3. – The total content of non-reactive silica, alumina and calcium oxide (labeled as $NRSiO_2$, $NRAl_2O_3$ and $NRCaO$) is calculated in the following manner:

$$NRSiO_2 = \frac{AF * 100 + U * 36.56}{100} = \frac{23.10 * 100 + 9.60 * 36.56}{100} = 26.61\%$$

$$NRAl_2O_3 = 0$$

$$NRCaO = \frac{U * 51.18 + R * 100}{100} = \frac{9.60 * 51.18 + 0.30 * 100}{100} = 5.21\%$$

Step 4. – The non-reactive silica, alumina and calcium oxide is subtracted from the total to obtain the reactive components labeled as $RSiO_2$, RAl_2O_3 and $RCaO$:

$$RSiO_2 = SiO_2 - NRSiO_2 = 37.77 - 26.61 = 11.16\%$$

$$RAl_2O_3 = Al_2O_3 - NRAl_2O_3 = 19.13 - 0 = 19.13\%$$

$$RCaO = CaO - NRCaO = 22.45 - 5.21 = 17.24\%$$

Table A.13 shows the values of $RSiO_2$, RAl_2O_3 and $RCaO$ for all the samples. The use of these values instead of the total values obtained from the XRF is expected to increase the accuracy of the model.

6.1.2. Relationship Between FA Characteristics and Compressive Strength of GPC

The values of $RSiO_2$, RAl_2O_3, $RCaO$, LOI, mean particle size in µm ($d50$), and specific surface area (SSA) were used as regressors and the compressive strength values as response. Three approaches were taken to develop the regression model: in the first approach the package LEAPS was used to perform subset selection; in the second approach the package LARS was used for simultaneous subset selection and coefficient optimization using the LASSO algorithm; and in the third approach the package GLMNET was used for subset selection and coefficient optimization using the EN algorithm. The models were built using 24 samples and validated with the remaining eight samples. LEAPS and LARS yielded similar values for the regression coefficients. However, the paths followed to choose the models were different. The values for the

coefficients given by the GLMNET package resulted in a model with a slightly higher mean square error than the first two and a slightly larger and variable departure from normality. An additional approach that attempted to simplify the input for the model was included. This "practical" model used of SiO_2, Al_2O_3 and CaO instead of $RSiO_2$, RAl_2O_3, $RCaO$ in an attempt to avoid the use of XRD analysis and simplify the process for GPC practitioners. However, the model showed low accuracy and poor sensitivity to changes in FA characteristics.

> ➤ *Approach 1 (Using LEAPS)*

LEAPS performed an exhaustive search of the best subsets of FA characteristics to predict the compressive strength. The results showed that $d50$ was the best regressor for a one variable model, RAl_2O_3 and $d50$ were the best regressors for a two variable model and $RSiO_2$, RAl_2O_3, and $d50$ for a three variable model. The best four-variable model did not include SSA and $RCaO$ and for the best five-variable model SSA was dropped.

The proposed subsets were evaluated in terms of: (1) adjusted R^2, which is typically preferred over the typical R^2 when comparing various models due to the fact that it penalizes models that have more regressors than they actually need, thus avoiding "over-fitting the model"; (2) variance inflation factor (VIF), a mean to quantify multicolinearity between variables. Regressors that exhibit VIF values greater than 10 are considered to be highly correlated, this can cause the model to give misleading results; and (3) mean squared error (MSE), a parameter that is generally regarded as a measure of the adequacy of the model, particularly useful in model building. A small MSE value is always preferred (Montgomery et al., 2006).

The model with the best adjusted R^2 value was the five-variable model where SSA was not included; it was labeled as Eq. (2):

$$f'_c = -3.68 + 0.59 * RSiO_2 + 3.35 * RAl_2O_3$$ (2)

$$-0.49 * RCaO - 0.74 * d50 - 4.40 * LOI \ (MPa),$$

where f'_c is the compressive strength of GPC after three days of thermal curing at 60°C. Eq. (2) had an adjusted R^2 of 0.72, an R^2 value of 0.78. Given the number of samples and regressors the R^2 value has a 95% confidence interval of $0.66 \geq R^2 \geq 0.90$. The MSE was 75.18 and the VIF values of the regressors were less than three; hence it was assumed there were no multicolinearity problems. The adequacy of Eq. (2) was analyzed using k-fold cross-validation where data is partitioned into k number of folds, $k - 1$ is used to create the model while the data in the remaining fold is used for validation, and the process is repeated k times with each fold being used once as the validation set. For example, in a three-fold cross-validation, two thirds of the total sample size (folds one and two) is used to create the model while the remaining third is used for validation (fold three); then folds two and three are used to create the model and fold one is used for validation; and finally folds one and three are used to create the model and fold two is used for validation. Figure 16 shows the cross-validation of Eq. (2) using two, three, four and five folds.
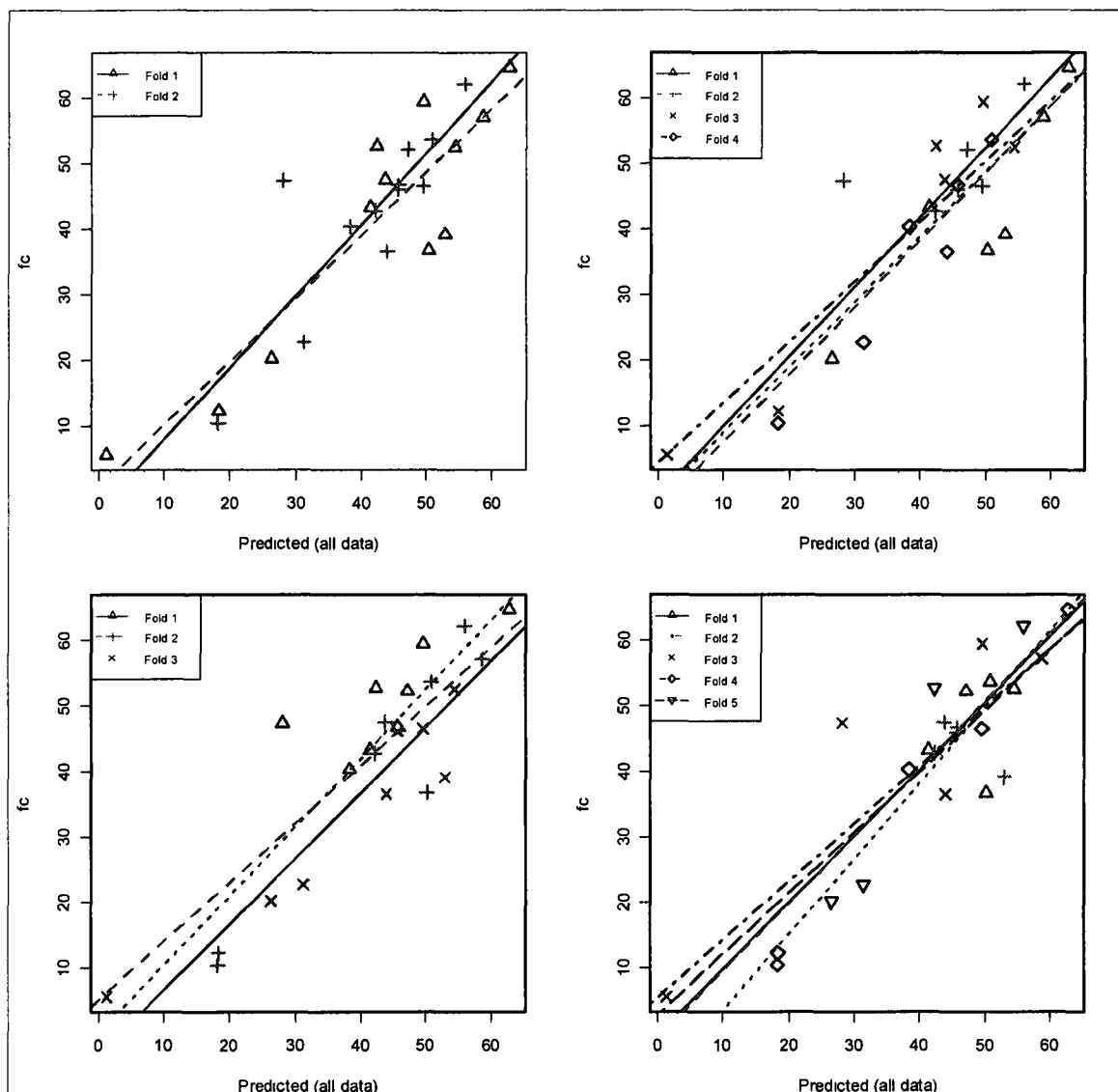
Figure 16 Cross-validation of Eq. (2) using two, three, four and five folds

The adequacy of Eq. (2) was further analyzed through residual analysis. Residual e_i refers to the difference between the fitted value $\hat{y}_i$ and the corresponding observation or experimental value y_i, $i = 1, 2,..., n$. Plotting residuals versus fitted values Montgomery et al. (2006) identified four cases that help to detect deficiencies in a regression model. Figure 17 shows residual vs. Fitted plots: (a) Satisfactory; (b) Funnel; (c) Double bow and (d) Nonlinear. Case (a) is the ideal where there are no evident defects in the model;

cases (b) and (c) indicate that the variance of the errors is not constant, which can be a problem since OLS works under the assumption of constant variance; and (d) suggests that the model is nonlinear and that the assumed relationship between the regressors and the response is not correct. In cases (b), (c) and (d) a transformation should be considered.
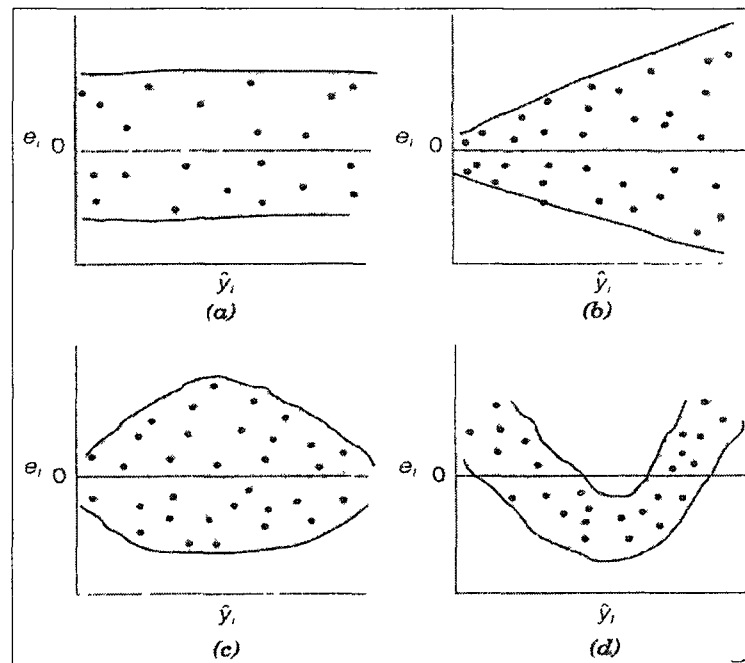
Figure 17 Residual vs. Fitted plots: (a) Satisfactory; (b) Funnel; (c) Double bow and (d) Nonlinear (Montgomery et al., 2006)

Figure 18 shows the analysis of Eq. (2) Residual vs. Fitted (top left), normal probability plot (bottom left), error of the model (top right) and validation using new data (bottom right). The residuals vs. Fitted values plot indicate that the double bow shape, case (c), could be present. This could be attributed to the nature of the collected data set where there are only six responses with values less than 35 MPa with the rest clustered towards the high end of the range. Hence, the weighted least squares technique and a

transformation of the regressors or the response are recommended in future work to improve the distribution of the residuals.
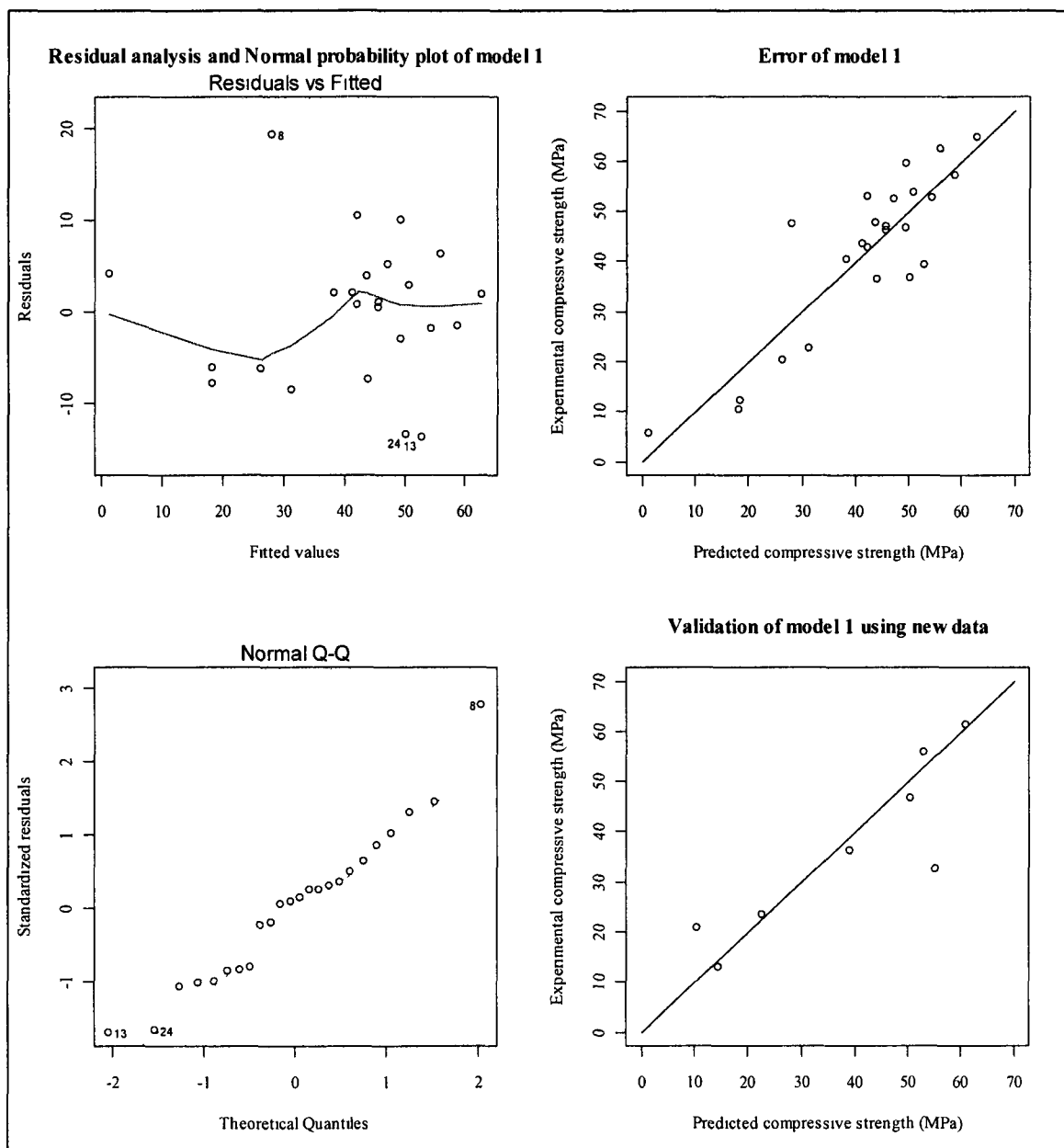
Figure 18 Analysis of Eq. (2) Residual vs. Fitted (top left), normal probability plot (bottom left), error of the model (top right) and validation using new data (bottom right)

Another assumption of the least squares technique is normality, the prediction and confidence intervals depend on this assumption. A normal probability plot (show in the

bottom left of Figure 18) was used to evaluate the normality of Eq. (2) by comparing its distribution with that of the dataset. In this plot the standardized residuals are plotted against the theoretical quantiles where in the ideal case of perfect normality the errors would lie along the dotted strait line.

The plot shows that the error distribution is slightly tailed indicating a small departure from normality. However, slight non-normality does not affect the model greatly (Montgomery et al., 2006). The top right of Figure 18 shows a graph of the predicted or fitted values vs. the observed compressive strength data. In this graph, as in the residuals plots, the eighth observation appears to have the largest error (approximately 19 MPa). The model predicts a value close to 28 MPa while the actual observation is 47 MPa. Three other observations had errors between 10 and 14 MPa and the rest less than 10 MPa, the average error was approximately 6 MPa.

Eq. (2) was validated using the remaining eight observations that were not used during the model building process. The bottom right of Figure 18 shows a plot of the predicted values versus the new compressive strength observations. In this case, the sixth observation was over-predicted by 23 MPa and the fourth observation was under-predicted by 10 MPa approximately. The rest of the observations had errors of less than 10 MPa. The error of Eq. (2) in the new dataset averaged 6 MPa approximately. The R code showing the model building process using LEAPS can be found in Appendix B.

➤ *Approach 2 (Using LARS)*

The LARS package performed variable selection and shrinkage simultaneously using the LASSO algorithm. The results showed nine steps where regressors were selected and their coefficients were shrunk. The subsets proposed in each of the nine

steps were evaluated in terms of residual sum of squares and Mallow's Cp. The model that exhibited the lowest Cp was found in the seventh step and similar to the model obtained by LEAPS kept all the variables except SSA. Herein, we refer to this model as Eq. (3):

$$f'_c = -3.62 + 0.59 * RSiO_2 + 3.35 * RAl_2O_3 \qquad (3)$$
$$-0.48 * RCaO - 0.74 * d50 - 4.39 * LOI \ (MPa).$$

Eq. (3) exhibited very similar coefficients as Eq. (2) with a Cp of 5.00 and MSE of 75.18. The R^2 of this model (0.78) was equal to the one obtained by LEAPS. However, the adjusted R^2 was 0.73, slightly higher than Eq. (2). Given the number of samples and regressors the R^2 value has a 95% confidence interval of $0.66 \geq R^2 \geq 0.90$. The VIF values were all below five. The adequacy of the model was analyzed through residual analysis. Figure 19 shows the analysis of Eq. (3): Linearization (top left), Validation using new data (bottom left), Residual vs. Fitted (top right), and Normal Probability plot (bottom right). The Residuals vs. Fitted plot appears to exhibit the "double-bow" shape as in case (c) of Figure 17. As stated before, this could be attributed to the nature of the collected data where there are very few data points in the low end of the compressive strength range. A transformation or the weighted least squares technique is recommended to verify the adequacy of Eq. (3). The normal probability plot appears to adhere well to normality and no evident problems can be identified from this graph.
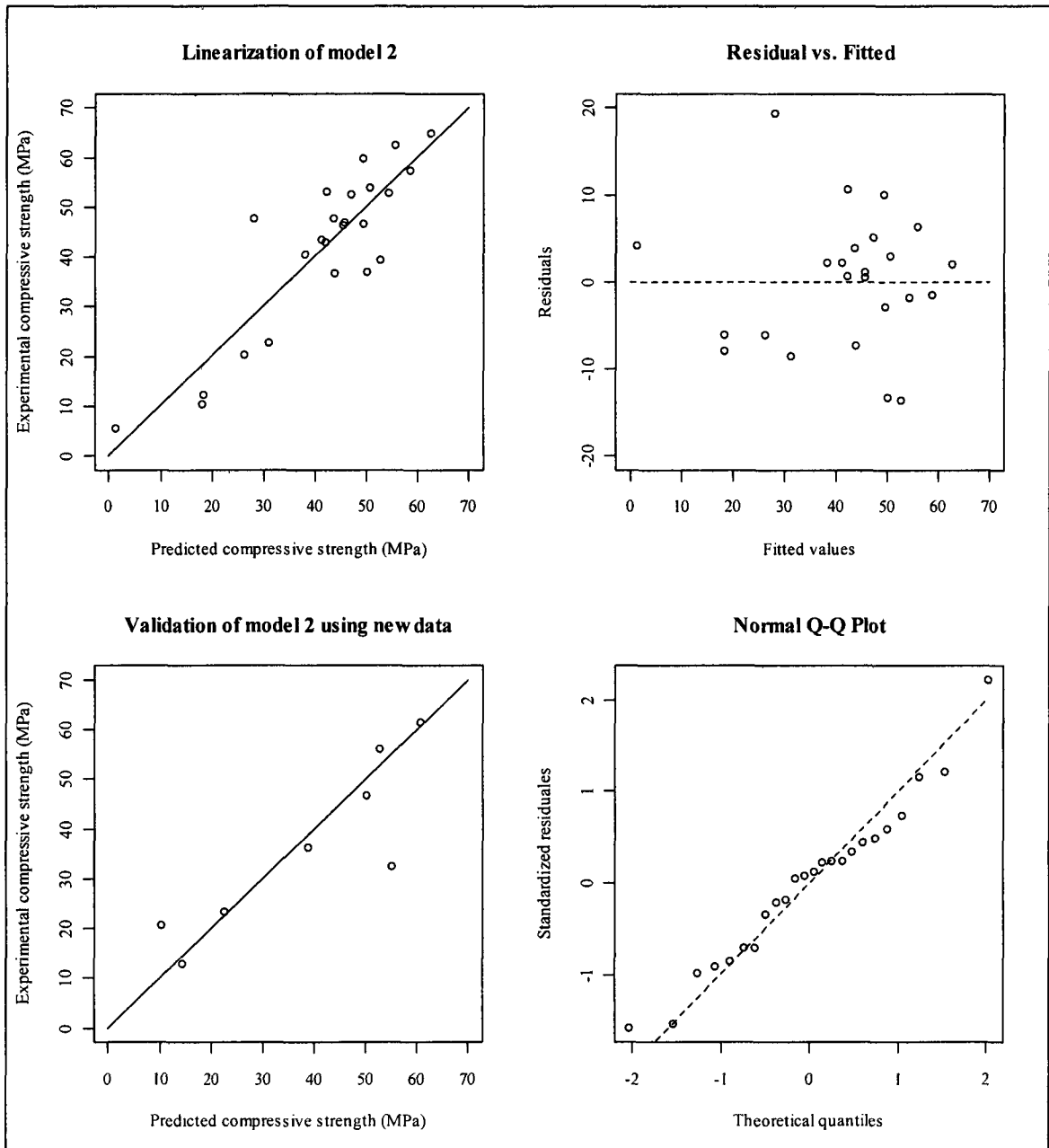
Figure 19 Analysis of Eq. (3) Linearization (top left), Validation using new data (bottom left), Residual vs. Fitted (top right) and Normal Probability plot (bottom right)

The coefficients of Eqs. (2) and (3) are very similar and therefore the error distribution is almost identical. Observation eight had the largest error, predicting approximately 19 MPa less than the actual value of 47 MPa. Another three observations

had errors between 10 and 14 MPa, the rest of the samples had errors of less than 10 MPa. The average error of Eq. (3) was 6 MPa approximately.

Eq. (3) was validated by using the remaining eight observations that were not used during the model building process. These results are presented in the bottom left of Figure 19. The sixth observation had the largest error (23 MPa approximately.), the fourth observation had an error of 10 MPa while the rest of the observations exhibited errors of less than 4 MPa approximately. The validation set had an average error of 6 MPa. The R code showing the model building process using LARS can be found in Appendix B.

➢ *Approach 3 (Using GLMNET)*

The package GLMNET performed variable selection and coefficient shrinking simultaneously using the EN algorithm which has two tuning parameters. The values for the tuning parameters were estimated through cross-validation to obtain the best performing model. The model obtained from using the best performing tuning parameters, like Eqs. (2) and (3), did not include the *SSA* variable and it was labeled as Eq. (4):

$$f'_c = 9.51 + 0.52 * RSiO_2 + 2.16 * RAl_2O_3 \qquad (4)$$
$$-0.066 * RCaO - 0.69 * d50 - 1.70 * LOI \ (MPa).$$

The MSE for Eq. (4) was 89.73, and the R^2 and adjusted R^2 values were 0.65 and 0.57, respectively, considerably less than Eqs. (2) and (3). Given the number of samples and regressors the R^2 value has a 95% confidence interval of $0.48 \geq R^2 \geq 0.82$. The VIF values were less than three indicating no signs of multicolinearity. The fit of Eq. (4) was assessed using residual analysis. Figure 20 shows the analysis of Eq. (4) Linearization (top left), Validation using new data (bottom left), Residual vs. Fitted (top right) and

Normal probability plot (bottom right). The residuals vs. fitted values graph shows a good distribution of the error variances, similar to case (a) of Figure 17. The normal probability plot shows a slight, but fluctuating departure from normality. Overall, there are no indications of deficiencies in the model.
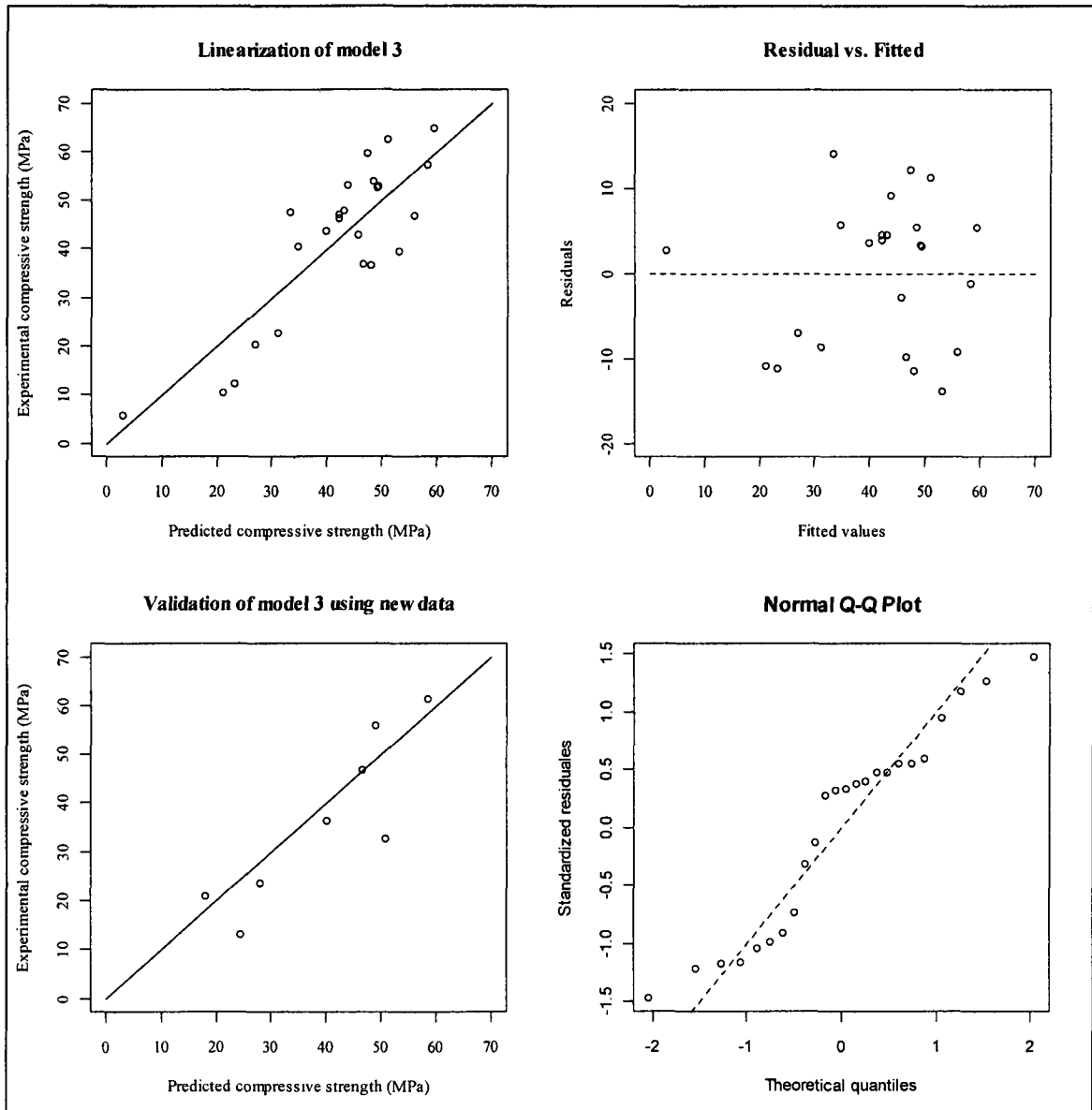
Figure 20 Analysis of Eq. (4) Linearization (top left), Validation using new data (bottom left), Residual vs. Fitted (top right) and Normal probability plot (bottom right)

As opposed to Eqs. (2) and (3), the largest error of Eq. (4) was 14 MPa, found in observations eight and 13. Observation eight exhibited a fitted value of 36 MPa and an experimental value close to 50 MPa and observation 13 showed a fitted value of 53 MPa and experimental value of 39 MPa approximately. Although, Eq. (4) had an average error of approximately 7 MPa, it exhibited a narrower error range (28 MPa) than the error range of 33 MPa found in these two approaches.

The validation of Eq. (4) using a new set of data shows that the largest error (found in the sixth observation) was 18 MPa over the actual experimental value. The fifth observation was also over-predicted by 11 MPa, while the rest of the observations had errors of less than 10 MPa. The average error of the validation dataset was 6 MPa approximately. The R code showing the model building process using GLMNET can be found in Appendix B.

➤ *Discussion of approaches one, two and three*

As stated above, LEAPS and LARS yielded very similar models with MSE of 75.18 MPa. However, LARS produced a model with slightly higher adjusted R^2 than LEAPS. Eqs. (2) and (3) presented acceptable distribution of residuals and no major departures from normality. GLMNET produced a model with higher MSE (89.73 MPa), lower R^2 and adjusted R^2 and its residual analysis showed no apparent deficiencies. Although the MSE of Eqs. (2) and (3) was smaller than the one of Eq. (4), the largest error of the first two was 19 MPa while in Eq. (4) the largest error was of 14 MPa. This shows that Eqs. (2) and (3) had larger errors but more observations were predicted on or close to the target, as opposed to Eq. (4) where the error span was smaller but the predictions had less accuracy. Given that the EN algorithm of GLMNET is believed to

perform well or better than the LASSO when the regressors are highly correlated, it was used due to potential multicolinearity in the dataset. However, the results from approaches one and two showed that there are no signs of multicolinearity between the regressors. In addition, GLMNET produced a model with less accuracy than the first two, thus it was not used in further analysis throughout this study. Packages LEAPS and LARS produced similar models, but due to its ease of use, LARS was chosen to perform *the rest of the multiple regression analysis in this study.*

The three approaches showed that *d50* had the strongest influence in the compressive strength of GPC followed by RAl_2O_3, *LOI*, $RSiO_2$ and finally *RCaO*. The three techniques discarded *SSA* during the model building process. The analysis of variance (ANOVA) of Eq. (3) is presented in Table 4 to illustrate how the statistical significance of each regressor was determined. The *P*-value was the parameter used to test the statistical significance of the regressors; the regressor with the lowest *P*-value (*d50*) is the most significant and the one with the highest value (*RCaO*) was the least significant. The parameters *d50* and *SSA* both describe physical characteristics of FA, in particular the packing of the particles. However, *d50* resulted highly influential, to the point that it may have hindered the impact that *SSA* exerts in the compressive strength. The parameters $RSiO_2$, RAl_2O_3 and *RCaO* were expected to have a positive sign in the equation since reactive silica and alumina are the main ingredients for the formation of geopolymer binder and it has been demonstrated that calcium also contributes to the compressive strength (Temuujin et al., 2009). A positive sign indicates that increasing these parameters would result in a direct increase in the compressive strength. However, while RAl_2O_3 exhibited a positive sign in the three models, $RSiO_2$ had a positive sign in

Eqs. (2) and (3) but not in Eq. (4). This can be attributed to one or more coefficients in Eq. (4) being calculated over their optimum values forcing $RSiO_2$ to drop its sign below zero to compensate for it. Similarly, $RCaO$ presented an unexpected negative sign in Eqs. (2), (3) and (4), most likely caused by the same phenomenon.

Table 4 ANOVA table of Eq. (3)

Parameter	Degrees of Freedom	Sum of Squares	Mean Square	F value	P
$RSiO_2$	1	444.91	444.91	5.9177	0.02564700
RAl_2O_3	1	1567.32	1567.32	20.8467	0.00024000
$RCaO$	1	0.88	0.88	0.0118	0.91482600
$d50$	1	2282.85	2282.85	30.3638	3.12×10^{-05}
LOI	1	539.24	539.24	7.1700	0.01534800
Residuals	18	1353.29	75.18		

The parameter $d50$ exhibited a negative sign in Eqs. (2), (3) and (4), and had the most significant impact in the compressive strength. This is in good agreement with research previously published by the author (Diaz et al., 2010; Diaz and Allouche 2010). Since the formation of geopolymer binder occurs only at the surface of the FA particles, FA with larger $d50$ provide less reaction surface and thus produce GPC with smaller compressive strength values.

The parameter LOI had a strong influence in the compressive strength exhibiting a negative sign throughout the three approaches. LOI is a measure of unburned carbon in FA, which has been demonstrated to cause problems in OPC-based concrete (Gao et al., 1997) as in GPC (Diaz et al., 2010). Although, the impact of unburned carbon in ordinary concrete is mainly in air entrainment while in GPC is in the liquid demand, recent studies performed by Hill and Folliard (2006) have shown that LOI may be inaccurate to quantify

the impact of carbon in concrete mixtures. The study showed that FA with low *LOI* in the form of fine carbon may have a greater impact in concrete than FA with high *LOI* in the form of larger carbon particles and/or perhaps with some of the carbon partially encapsulated in glass, yet this still has to be proven for GPC. This phenomenon was observed during this investigation as some FA samples, in spite of having high *LOI* contents, exhibited low liquid demands and average compressive strength.

➤ *A practical and economical approach*

A potential application of this study can be the use of the proposed equations for quality assurance and control in commercial production of GPC. The quality of FA for GPC production can be monitored by determining the *LOI*, mean particle size, reactive silica, alumina and calcium oxides and plugging them into Eq. (3) to calculate its potential compressive strength. Variability of FA characteristics and its resulting impact in the potential compressive strength of GPC can be quantified following this procedure. However, the qualitative and quantitative analysis through X-ray diffraction can be a complex process, many times dependant on the criteria of the technician performing the analysis for the indexation of phases and as a consequence it may not be practical for monitoring commercial production. Furthermore, the determination of reactive silica, alumina and calcium oxides can be a tedious and somewhat time-consuming process. Therefore, a model that uses the total silica, alumina and calcium oxides from the chemical analysis rather than its reactive components determined by X-ray diffraction was developed:

$$f'_c = 16.22 + 1.33 * SiO_2 - 0.78 * Al_2O_3 + \qquad (5)$$

$$0.71 * CaO - 0.90 * d50 \ (MPa).$$

The adjusted R^2 value of this model was 0.63 and the R^2 value 0.70, considerably less than Eq. (3). Given the number of samples and regressors the R^2 value has a 95% confidence interval of $0.54 \geq R^2 \geq 0.86$. The VIF values of SiO_2 and CaO were 5.74 and 5.39; slightly higher than the recommended range of zero to five (Montgomery et al., 2007) indicating that SiO_2 and CaO may be moderately correlated. Conversely, Kutner et al. (2004) proposed a maximum value of 10 instead of five to detect multicolinearity problems. The VIF values obtained for this model fall within the acceptable range of the latter. It is worth noting that the coefficient for Al_2O_3 appears with a negative sign in the equation implying that it was detrimental to the compressive strength of GPC. This premise is contrary to the theoretical chemistry fundamentals behind the regression model where alumina plays an essential role in the formation of geopolymer gel, thus it is assumed to have a positive effect. This can be an indication that one or more of the rest of the coefficients are larger than their optimum value and the coefficient of Al_2O_3 decreases its value in an attempt to compensate for it.

Figure 21 shows the analysis of Eq. (5): Residual vs. Fitted (top left), normal probability plot (bottom left), linearization (top right), and validation using new data (bottom right). The residual vs. fitted plot showed that the variance of the residuals appears to have the double-bow shape as case (c) of Figure 17, indicating that the assumption of constant variance might be compromised. However, as stated before, this deficiency could be a result of the nature of the collected data where there are few samples in the low end of the compressive strength range and the remaining samples are clustered in the mid to high end of the range.
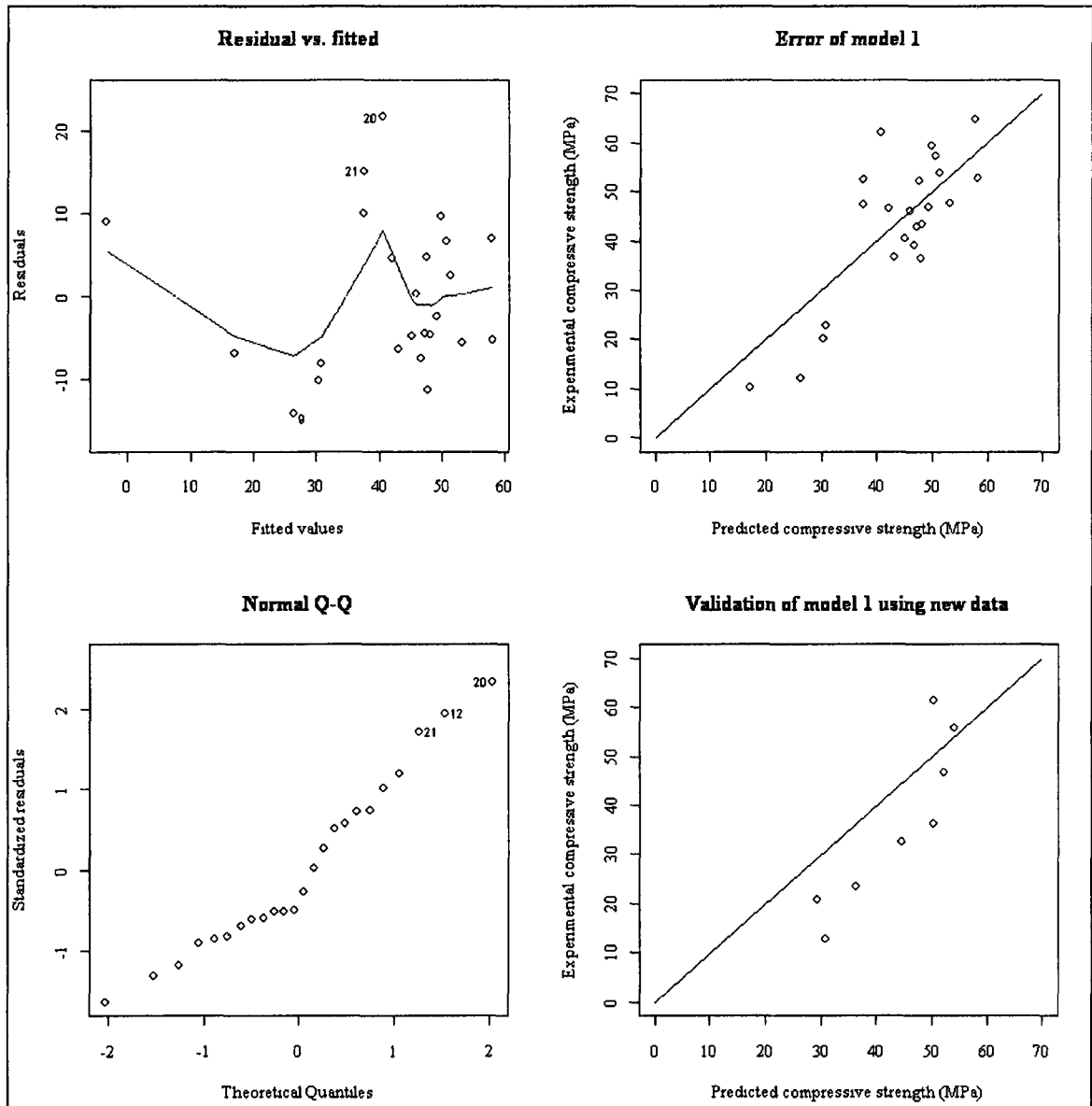
Figure 21 Analysis of Eq. (5) Residual vs. Fitted (top left), Normal Probability plot (bottom left), Linearization (top right), and Validation using new data (bottom right)

The normal probability plot shows that that the model adheres well to normality. The graph showing the error of the model is indicative that although, Eq. (5) is more practical and applicable than Eq. (3), it has less accuracy. The maximum error found for this model was 22 MPa, four observations had errors between 11 and 14 MPa and the rest

of them presented errors of less than 10 MPa. The average error for the 24 observations was of 8 MPa approximately.

The model was validated using eight new observations; the results are shown in the bottom right of Figure 21. The regression model predicted the compressive strength of the validation set with an average error of 10 MPa, and with a maximum error of 18 MPa approximately. The regressors on which this model is based, particularly SiO_2, Al_2O_3 and CaO, serve to represent the true underlying chemical and physical interactions in a rather crude manner as it is known that only a part of them is reactive while the rest stays inert throughout the reaction and this reactive material varies depending on the amorphous-crystalline ratio and type of crystalline phases present in FA. Therefore, the reduced accuracy of the Eq. (5) concurs well with the chemical and crystallographic fundamentals behind the regression models. The R code showing the model building process for Eq. (5) can be found in Appendix B.

6.1.3. FA Characteristics vs. Density of GPC

The physical characteristics of FA were compared against the density of GPC to identify any possible correlations. It was found that the specific gravity of FA had the strongest correlation with the resulting concrete density. The regression model obtained from the analysis was:

$$w = 2649 - 1979 * \frac{1}{SG^2} \ (kg/m^3), \tag{6}$$

where w represents the density of GPC as per ASTM standard C 138 and SG is the specific gravity of FA determined following ASTM standard C 188. Eq. (6) had an R^2 value of 0.76 with a 95% confidence interval of $0.61 \geq R^2 \geq 0.91$. A plot of SG vs. w that includes a graphical representation of the equation is presented in Figure 22.
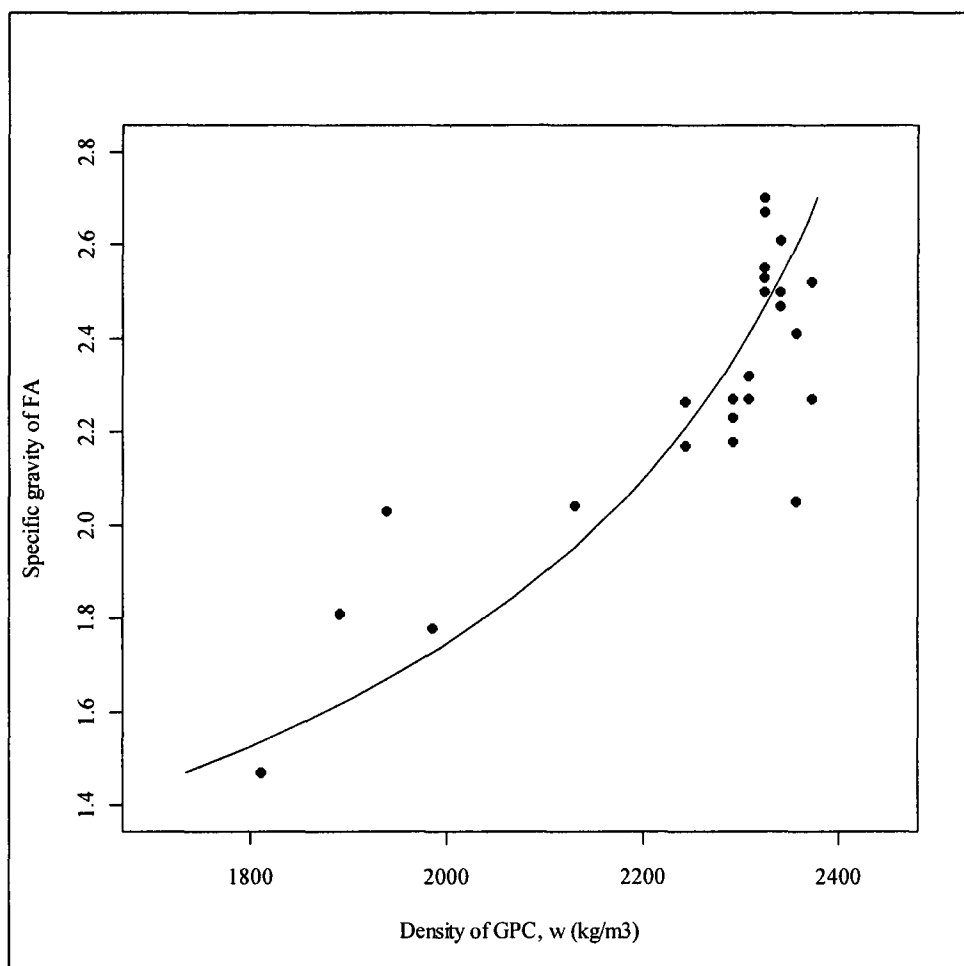
Figure 22 Regression model of FA specific gravity vs. density of GPC

The residuals of Eq. (6) were analyzed and no major deficiencies were found. The model converged well with normality and the residuals showed no apparent defects. The largest error was 231 kg/m³ over the value of its corresponding observation. Eq. (6) predicted an average of 55 kg/m³ off target. In general terms, Eq. (6) tended to over-predict at low specific gravity values and under-predict at the higher end of the values. However, the prediction accuracy seems to increase at higher *SG* values. This could be an indication that another variable was needed in order to predict GPC density more accurately. As in Section 6.1.2., the model was built using 24 observations and validated

with the remaining eight; the results of the validation of the regression model of FA specific gravity vs. density of GPC are shown in Figure 23. The average error was approximately 31 kg/m^3 indicating that the fitted values laid close to their corresponding observation.
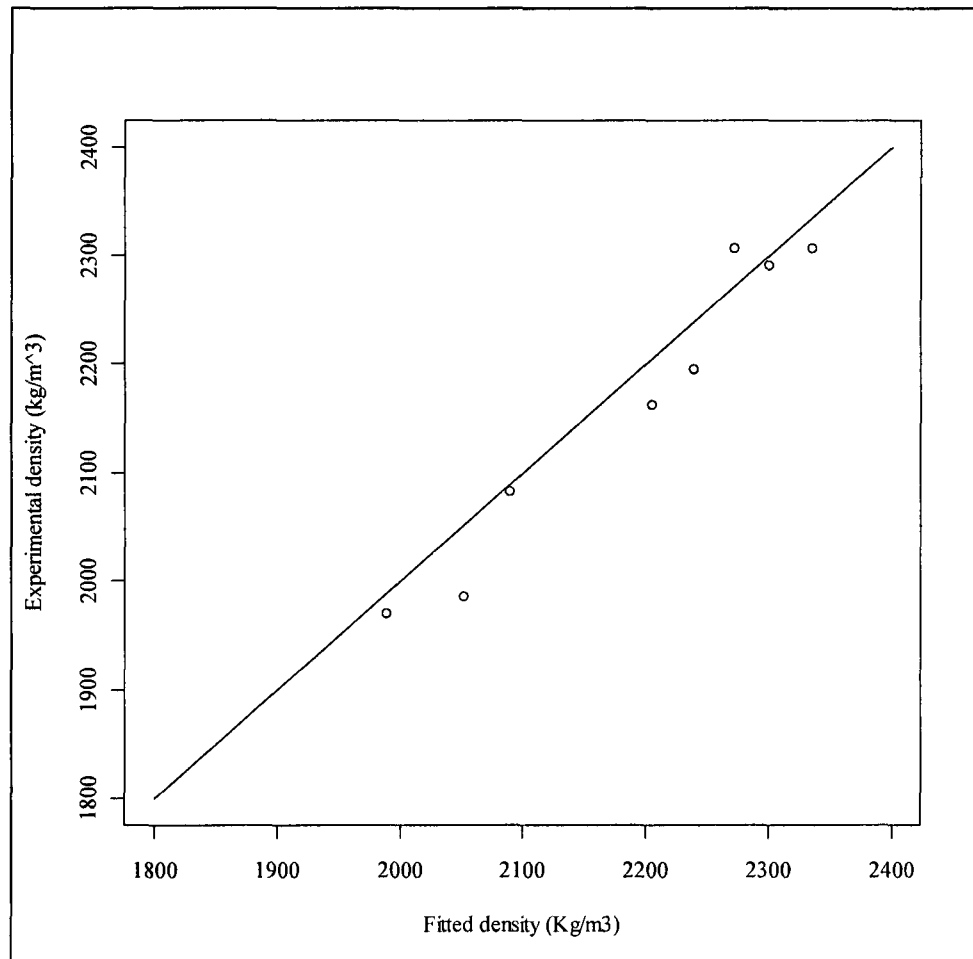
Figure 23 Validation of the regression model of FA specific gravity vs. density of GPC

It can be presumed that the relationship between the density of GPC and the specific gravity of FA is merely physical. As opposed to OPC concrete, GPC cannot convert water into a solid and reduce the pore volume through the hardening process (Provis et al., 2010). Therefore, the packing characteristics of FA have a direct and

significant impact in the liquid demand of GPC. FA with low specific gravity values demands more liquid to fill larger voids caused by poor packing resulting in a higher pore volume and thus lowers density in fresh GPC. Ultimately, the pore volume and density of GPC are expected to impact the stiffness of the material.

6.1.4. FA Characteristics vs. Setting Time of GPC

The preliminary tests presented in Chapter 3 showed that setting time of GPC is strongly influenced by the calcium content in FA. This premise remained true throughout the rest of this study, as samples were added into the database they followed the same trend. A scatter plot of setting time vs. reactive calcium oxide is shown in Figure 24. It can be seen that the setting time decreases as the $RCaO$ content increases in a manner somewhat similar to an exponential decay curve. This can be attributed to the calcium in the mixture reacting with the silicate and aluminates monomers dissolved from the source material, forming CSH and CASH. The hydration of these compounds results in water deficiency and thus raises the alkalinity of the mixture. The increase in alkalinity promotes higher and faster dissolution of silicate and aluminate species from the source material, and consequently an increased rate of polycondensation/geopolymerization. Thus, the presence of calcium contributes to the mechanical strength of geopolymer concrete not only by forming CSH and CASH, but also via the enhancement of the geopolymerization process. However, the "enhanced geopolymerization" and the nucleation sites created by the precipitated CSH and CASH lower the setting time (Temuujin et al., 2009).
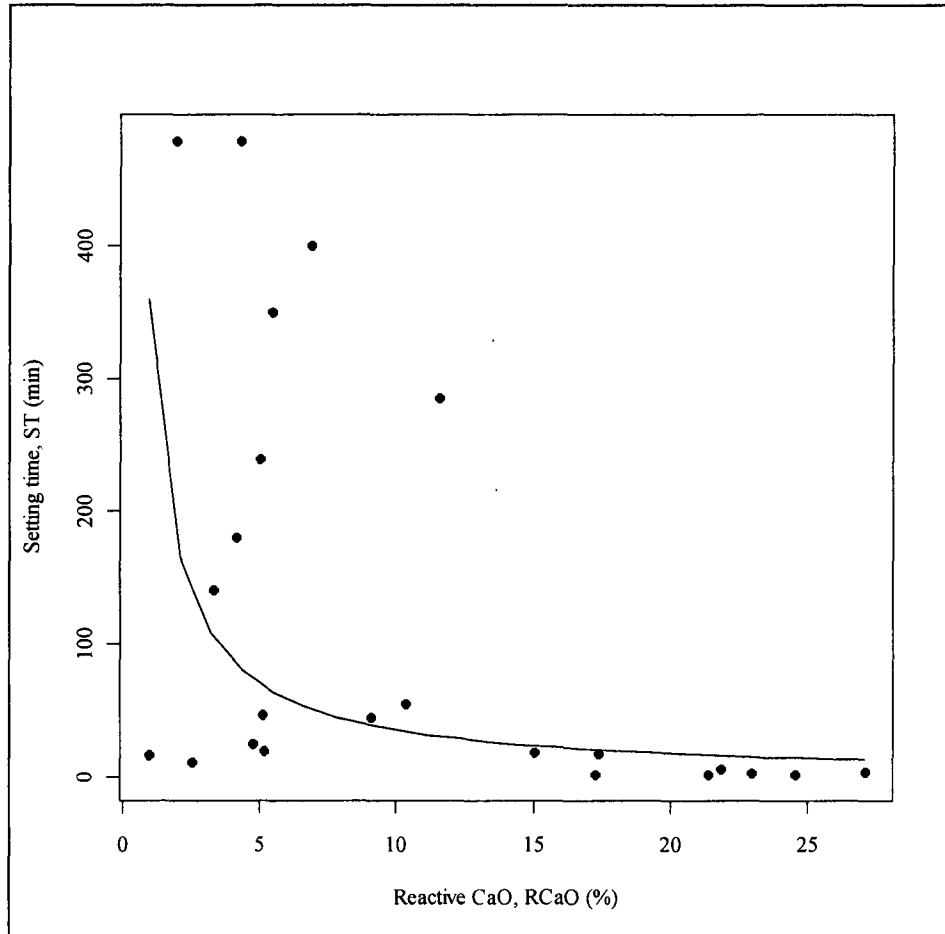
Figure 24 Scatter plot of GPC setting time vs. reactive CaO content

Despite the evident relationship between *RCaO* and the setting time of GPC it was not possible to propose a regression model that captures this interaction due to an excessive dispersion of some points between 0 and 12% *RCaO*. For example, several observations that had approximately 5% *RCaO*, yet exhibited setting times ranging from 25 to 480 minutes. This can be an indication that although *RCaO* and setting time are inversely related, their interaction may be more complex and possibly other factors that impact the setting time were not taken into account.

6.2. Analysis of the Mechanical Properties of GPC

6.2.1. Compressive vs. Flexural Strength

Figure 25 shows a scatter plot of the compressive versus the flexural strengths as well as a regression model representing the relationship between the two variables. The proposed regression model is:

$$f_r = 0.68\sqrt{f'_c}\,(MPa), \tag{7}$$

where f_r is the flexural strength and f'_c is the compressive strength after three days of thermal curing at 60°C. The model, labeled as Eq. (7), presented an R^2 value of 0.72 with a 95% confidence interval of $0.55 \geq R^2 \geq 0.89$, was obtained using the least squares technique and was found to best "fit" the experimental data after analyzing residuals and R^2 values of several different regression models. Eq. (7) seems to accurately predict the flexural strength using the compressive strength values despite the fact that the observations were recorded from different batches. To support the validity of the model, data reported by Fernandez-Jimenez et al. (2006) and Sofi et al. (2007) was also included. It is worth noting that this experimental model for GPC is similar to the equation given by the American Concrete Institute in the Building Code 318-08 in Section 8.5.2.3 to estimate the modulus of rupture for use in calculating deflections (ACI, 2008):

$$f_r = 0.62\sqrt{f'_c}\,(MPa), \tag{8}$$

where f_r is the tensile flexural strength and f'_c is the compressive strength of OPC concrete after 28 days of curing.
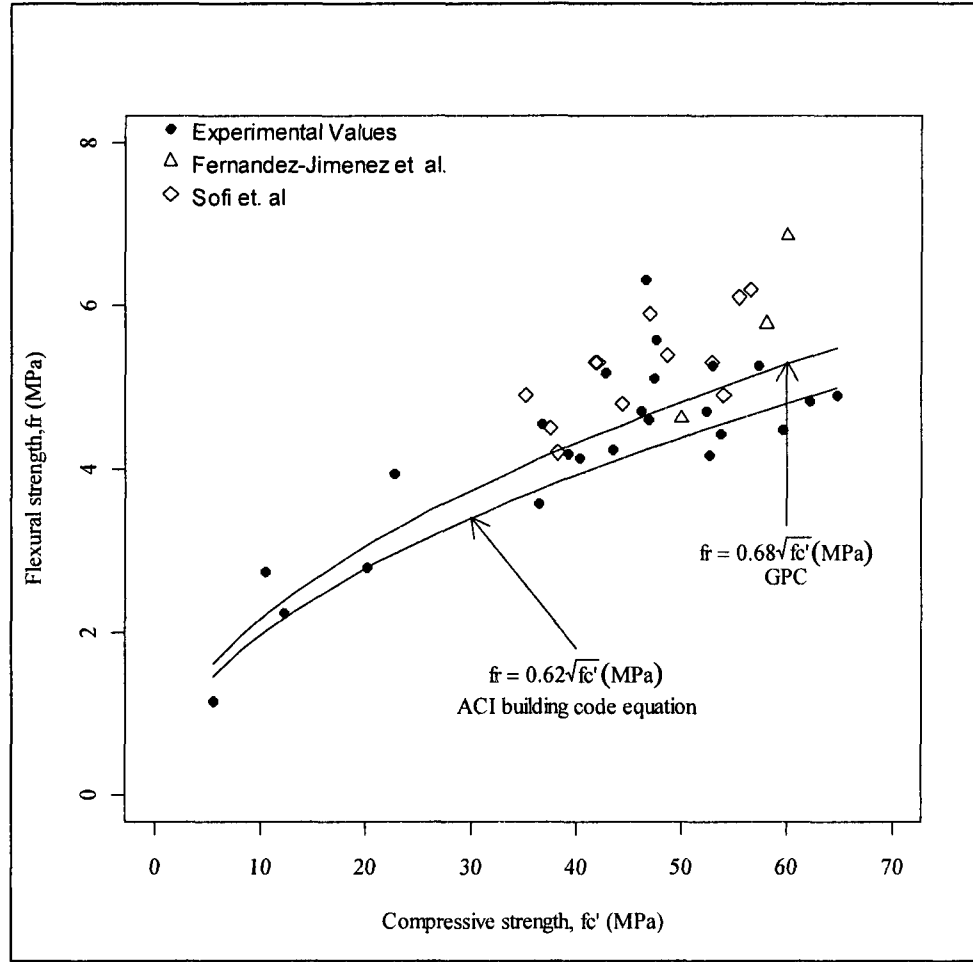
Figure 25 Flexural vs. compressive strength

The adequacy of Eq. (7) was assessed by analyzing the residuals. They seemed to adhere well to case (a) of Figure 17 indicating a constant variance of the errors and the normal probability plot showed no signs of normality problems. The largest error was 1.66 MPa, with the model predicting a value of 4.65 MPa, but the corresponding observation having a value of 6.31 MPa. The rest of the observations yielded errors of less than 1 MPa. The fitted values had an average error of 0.47 MPa. Eq. (7) was further evaluated using eight new observations; the results are presented in Figure 26. Eq. (7)

predicted the flexural strength as a function of the compressive strength with less than 1

MPa of error and an average of 0.6 MPa.
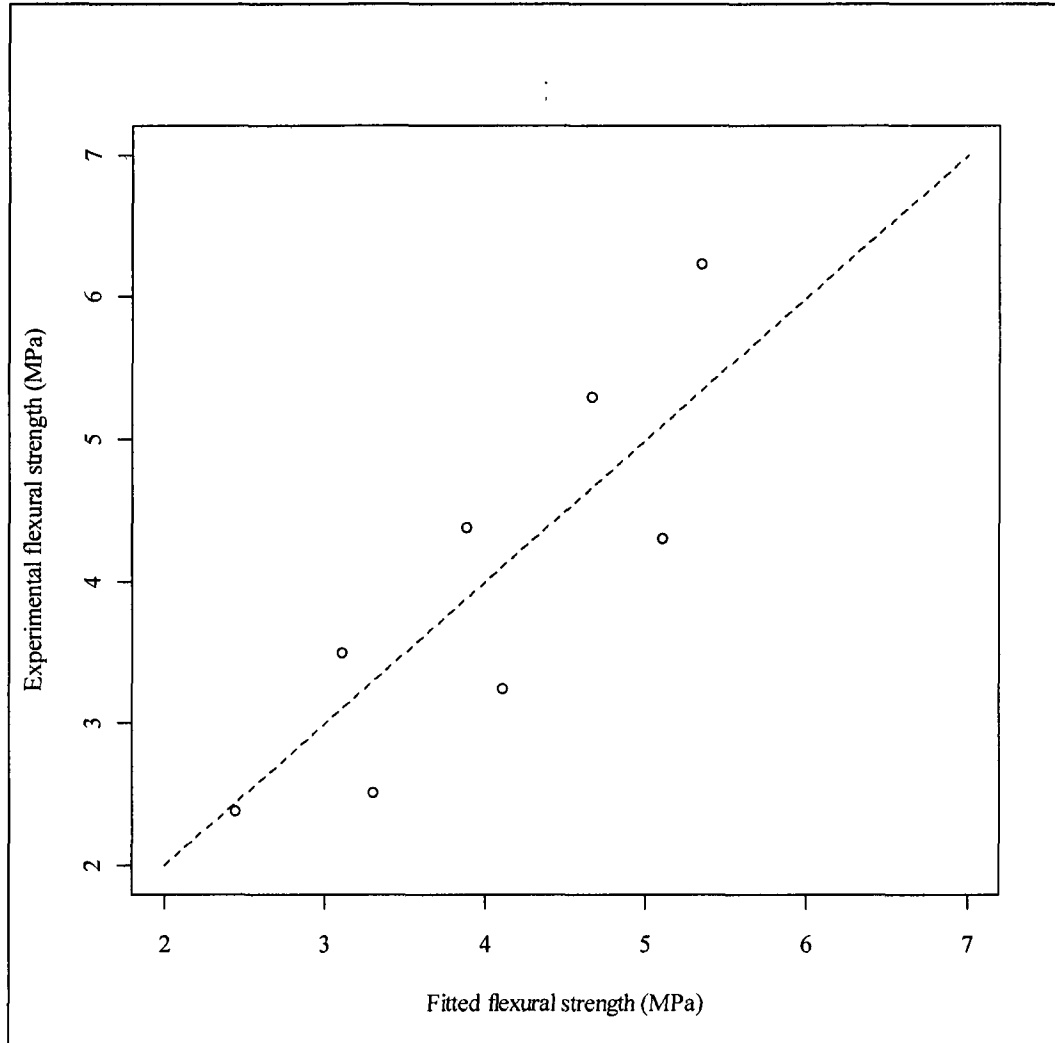
Figure 26 Validation of the compressive vs. flexural strength regression model

6.2.2. Compressive vs. Static
Elastic Modulus

A regression model representing the correlation between static elastic modulus

and compressive strength is presented in Figure 27. The equation obtained from the

analysis is:

$$E_c = 580f'_c \ (MPa),$$ (9)

where E_c is the static elastic modulus and f'_c is the compressive strength. The R^2 value for this model, which was labeled as Eq. (9), was 0.81 and had 95% confidence interval of $0.68 \geq R^2 \geq 0.94$. To support the validity of the proposed regression model data reported by Fernandez-Jimenez et al. (2006) and Sofi et al. (2007) was also included. ACI 318 (2008) in Section 8.5.1. suggests the following expression for computing the modulus of elasticity for normal weight concrete as:

$$E_c = 4733\sqrt{f'_c} \ (MPa).$$ (10)
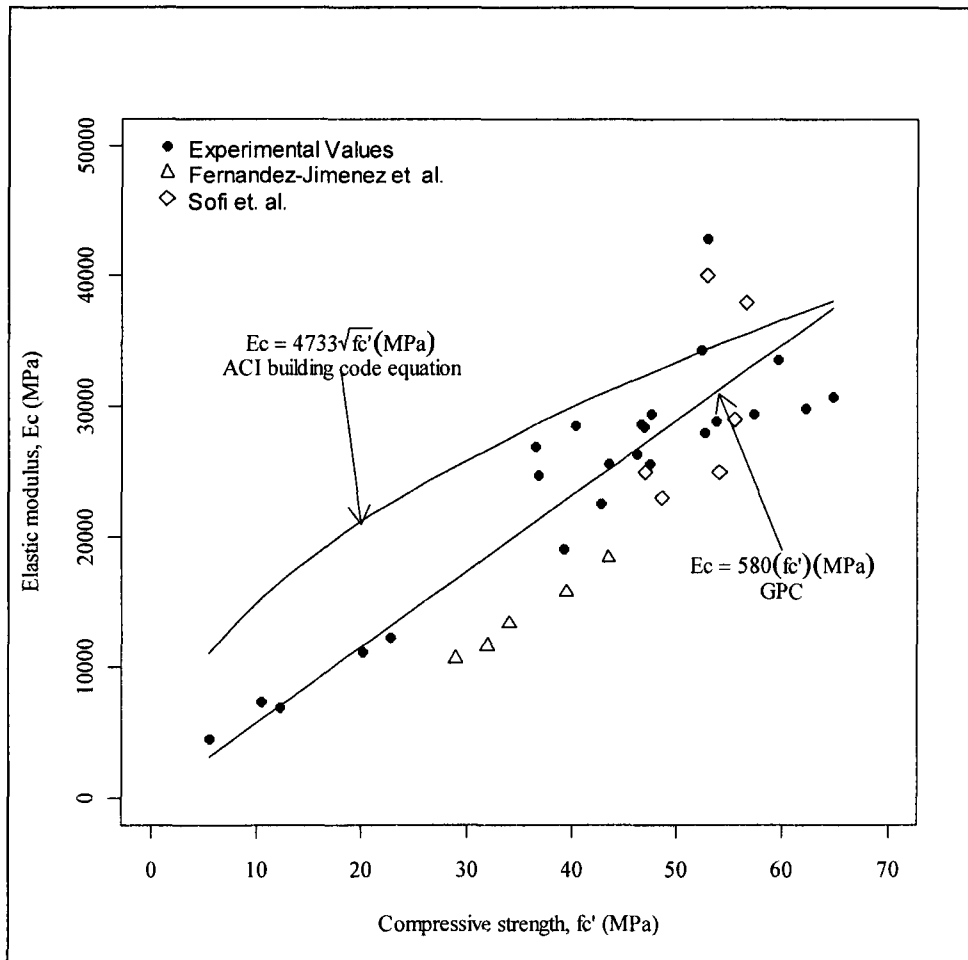
Figure 27 Static elastic modulus vs. compressive strength

However, the GPC samples tested during this study exhibited a wide range of density values and most concrete professionals are familiar with a square-root functional form to represent this relationship, thus another regression model, labeled as Eq. (11), was derived using compressive strength and density of GPC as predictors of elastic modulus:

$$E_c = 0.037(w)^{1.5}\sqrt{f'_c}(MPa),\qquad(11)$$

where w is the density of GPC in kg/m^3 and the f'_c values are expressed in MPa. This model exhibited an R^2 value of 0.83 with a 95% confidence interval of $0.72 \geq R^2 \geq 0.94$ suggesting that the inclusion of density in the prediction model helps in capturing the variability of the elastic modulus of GPC. Eq. (11) was found to predict the elastic modulus using the density and compressive strength values with reasonable accuracy despite the fact that some of the density values were recorded from a different batch. In addition the model presented in Eq. (11) adhered closer to normality and had a better distribution of residuals than the model presented in Eq. (9). The applicability of the model was supported by including data previously reported by Sofi et al. (2007). A similar equation is given in ACI 318 (2008) Section 8.5.1, which was derived from short-term tests of OPC concrete ranging in density from 1,442 to 2,483 kg/m^3:

$$E_c = 0.043(w)^{1.5}\sqrt{f'_c}(MPa).\qquad(12)$$

Figure 28 shows a plot comparing Eq. (11) and (12). An outlier seems to be present in the regression model given in Eq. (11); an observation with an error of approximately 13,000 MPa while the rest of the observations yielded residuals of less than 6,000 MPa approximately. The average error was 2,869 MPa. Eq. (11) was validated, as the rest of the models developed during this study, using the eight

observations that were not included in the model building process. Here, it was observed that the model tends to slightly over-predict at low elastic modulus values and to under-predict at higher values. However, this conjecture may be premature since the validation set is relatively small, and to confirm it more observations would be required.
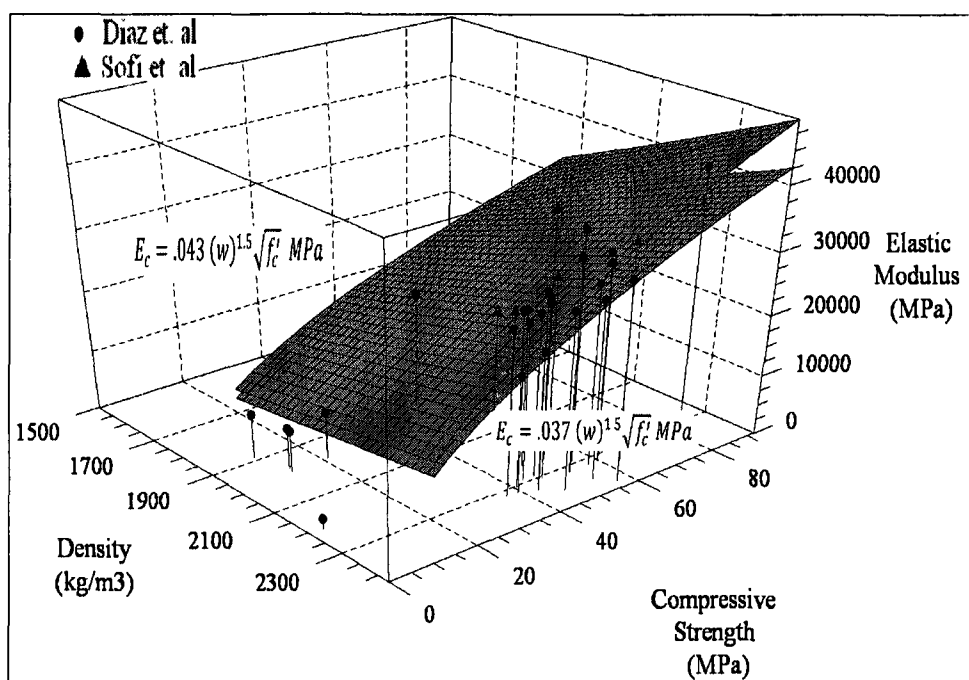
Figure 28 Elastic modulus as a function of density and compressive strength

6.2.3. Discussion of the Mechanical Properties

This study proved that relationships exist among the compressive strength, density, elastic modulus and flexural tensile strength of GPC that are similar to those observed for ordinary concrete. It can be inferred from Eq. (6) that as the compressive strength increases so does the flexural strength; however the ratio of flexural to compressive strength decreases as the compressive strength increases. Eq. (6) is comparable to Eq. (7) from ACI 318 (2008) Section 8.5.2.3 for OPC concrete, except the expected values of the flexural strength are slightly higher than those obtained for OPC as

can be seen in Figure 25. From Figure 25 it can also be appreciated that the vast majority of data points previously reported by Fernandez-Jimenez et al. (2006) and Sofi et al. (2007) adhere well to Eq. (7) increasing its reliability.

Similarly to ordinary concrete, the elastic modulus of GPC is influenced by the elastic modulus of the geopolymer paste and the elastic modulus of the aggregate. Increasing the activator solution to FA ratio increases the porosity of the paste and consequently decreases the elastic modulus and strength of the GPC. Since the aggregates and the mix design were kept constant for all specimens, variations in the elastic modulus of the aggregates can be considered to have negligible effect on the elastic modulus of the resulting geopolymer concrete. Therefore, variations in the elastic modulus of GPC can be attributed mainly to variations in the elastic modulus of the geopolymer paste. Eq. (9) explains the relationship between the elastic modulus and the compressive strength, which follows a positive linear relation. The equation that ACI 318-08 puts forward to express the variation of the elastic modulus of ordinary concrete as a function of the compressive strength for normal weight concrete, namely Eq. (10), follows a similar pattern, however the elastic modulus to compressive strength ratio decreases as the compressive strength increases, while in GPC this ratio remains constant. The data reported by Fernandez-Jimenez et al. (2006) and Sofi et al. (2007), as can be seen in Figure 27, follows the same trend as Eq. (9). Given that the density values of the GPC samples varied depending on the FA's physical characteristics, Eq. (11) was found to be a statistically valid method for determining the elastic modulus as a function of compressive strength and density of the GPC. When compared with Eq. (12) from ACI 318 (2008) for ordinary concrete, there is a striking similarity between the two

expressions. In Figure 28 it can be seen that the elastic modulus values increase as the density increases. High density values are indicative of low porosity and thus a reduced void system in the concrete which increases the stiffness of the material.

Poisson's ratio values of ordinary concrete can range from 0.11 to 0.21 but usually fall in the range from 0.15 to 0.20 (MacGregor and Wight, 2005). Values obtained for the GPC samples, which averaged 0.14, tend to populate the lower end of this range. However, considering that the compressive strength of the majority of GPC samples surpasses 41 MPa, the lower limit defining "high strength concrete" (MacGregor and Wight, 2005), Poisson's ratio values of GPC are in good agreement with values expected for high strength concrete.

6.3. Testing the Models

The accuracy of the overall statistical analysis was further evaluated by using the optimum model to predict compressive strength, which was Eq. (3), Eq. (6) to predict density of GPC, and then using this predicted values to calculate the flexural strength and the elastic modulus using Eqs. (7) and (11) as proposed in Sections 6.2.1. and 6.2.2. In other words, using the chemical, crystallographic and physical characteristics of the FA, the potential compressive strength, density, flexural strength and elastic modulus of GPC were predicted using the equations proposed in this study. The results are summarized in Table 5. The errors associated with the density and compressive strength are dependant of the accuracy of the models. However, the flexural strength, and elastic modulus values were calculated using the predicted density and compressive strength values, i.e., they are subject to the error related to the prediction of density and compressive strength and the

error related to equations used to predict flexural strength and elastic modulus. Yet, the predictions are fairly accurate.

Table 5 Summary of statistical results 1

Sample	w (kg/m3)			f'_c (MPa)			f_r (MPa)			E_c (MPa)		
	O	P	E	O	P	E	O	P	E	O	P	E
3	2291	2300	9	55.89	53.01	2.88	4.3	4.95	0.65	37108	29706	7402
6	2307	2272	35	46.69	50.45	3.76	5.3	4.83	0.47	29358	28454	904
17	2307	2335	28	61.38	61.01	0.37	6.23	5.31	0.92	31447	32605	1158
13	1986	2052	66	20.68	10.46	10.22	3.5	2.2	1.3	7960	11121	3161
12	1970	1988	18	12.82	14.47	1.65	2.38	2.59	0.21	6812	12471	5659
28	2083	2089	6	32.45	55.23	22.78	4.38	5.05	0.67	22808	26255	3447
31	2163	2204	41	36.24	39.17	2.93	3.25	4.26	1.01	21456	23969	2513
29	2195	2238	43	23.36	22.79	0.57	2.52	3.25	0.73	13176	18705	5529
Avg E	30.75			5.645			0.745			3722		

O = Observed Value E = Error
P = Predicted Value

Table 6 shows a similar summary but the predictions are based on the Eq. (5). As discussed before Eq. (5) is much less sensitive to changes of FA characteristics and tends to over predict most of the validation values. Comparing Tables 5 and 6, it can be seen that the average prediction error of Eq. (5) is approximately three times greater than the one exhibited by Eq. (3). The same tendency applies for the prediction errors of the elastic modulus and the flexural strength where the average errors of Eq. (5) are significantly greater than those of Eq. (3). Thus, Eq. (5) cannot be recommended to evaluate the potential of FA as source material for GPC.

Table 6 Summary of statistical results 2

Sample	w (kg/m3)			f'c (MPa)			fr (MPa)			Ec (MPa)		
	O	P	E	O	P	E	O	P	E	O	P	E
3	2291	2300	9	55.89	65.08	9.19	4.3	5.49	1.19	37108	32916	4192
6	2307	2272	35	46.69	64.25	17.56	5.3	5.45	0.15	29358	32110	2752
17	2307	2335	28	61.38	57.99	3.39	6.23	5.18	1.05	31447	31788	341
13	1986	2052	66	20.68	40.82	20.14	3.5	4.34	0.84	7960	21966	14006
12	1970	1988	18	12.82	42.09	29.27	2.38	4.41	2.03	6812	21275	14463
28	2083	2089	6	32.45	56.09	23.64	4.38	5.09	0.71	22808	26459	3651
31	2163	2204	41	36.24	61.72	25.48	3.25	5.34	2.09	21456	30087	8631
29	2195	2238	43	23.36	46.54	23.18	2.52	4.64	2.12	13176	26729	13553
Avg E	30.75			18.98			1.27			7699		

O = Observed Value   E = Error
P = Predicted Value

CHAPTER 7

CONCLUSIONS AND FUTURE WORK

7.1. Conclusions

This manuscript puts forward a database of XRD analysis, chemical composition and particle size distribution performed on 32 FA stockpiles collected from different coal-fired power generating stations around the US. The potential for GPC production from each FA stockpile was compared and a statistical analysis was performed to identify and quantify the major causes of variation that impact the mechanical properties of FA-based geopolymer concrete, namely; silica, alumina, calcium and *LOI* as well as the amorphous content and fineness. As the true reaction mechanism through which geopolymer binders are formed is still debated and not well understood, a set of regression models that attempt to explain the true underlying mechanism are put forward. Eq. (3) was found to be the best regression model to predict the compressive strength of GPC, it uses reactive silica, alumina and calcium oxide (as determined in Section 6.1.1.) as well as *LOI* and the mean particle size as regressors. It showed to be the best fit by predicting compressive strength with an average accuracy of ± 6 MPa, having an adjusted R^2 value of 0.73 and an R^2 of 0.78.

Eq. (5), an alternative model to predict the compressive strength, was tested in an attempt to simplify the input of the model for GPC practitioners and avoid the calculation of reactive silica, alumina and calcium oxide. For Eq. (5), the totals were used instead of

the reactive components. The resulting model predicted the compressive strength with an average accuracy of 8 MPa. However, the errors were significantly dispersed and it showed reduced sensitivity to changes in FA characteristics. This was confirmed in its poor performance to predict the compressive strength values of the validation data (Table 5).

The chemical rationale behind the aforementioned models is that silica and alumina are the main precursors for geopolymer binder formation and these are assumed to dissolve from FA in a highly alkaline solution and then recombine using sodium as a charge-balancing agent to form geopolymer gel (Davidovits, 1993). Calcium in FA is believed to enhance the mechanical strength not only by forming hydration products in parallel to geopolymer but also by raising the alkalinity as water is consumed by the hydration reactions (Temuujin et al., 2009; Diaz et al., 2010). However, not all silica, alumina and calcium participate in this reactions as some are typically combined in a quasi-inert crystalline arrangement. Therefore, in Eq. (3) the molecules combined in a crystalline form were assumed to be inert and only the reactive components were taken into account for the calculations. Conversely, Eq. (5) used the total silica, alumina and calcium oxide for the calculations. The relatively high prediction accuracy of Eq. (3) compared to Eq. (5) can be attributed to this difference.

The *LOI* content and the mean particle size were also found to influence the compressive strength. Their influence can be attributed to physical interactions that affect the reaction kinetics. *LOI* (unburned carbon) was found to have an adverse effect in the mechanical strength of GPC due to its hygroscopic nature that causes a higher liquid demand. However, its effect on GPC may vary depending on its fineness and reactivity.

For example, a small amount of highly fine carbon may have a more pronounced effect than a high amount of coarser carbon. The influence of the mean particle size in the compressive strength of GPC can be attributed to the rate of dissolution of silicon, aluminum and calcium species from the FA. Since it is believed that the geopolymerization reaction occurs only at the particle-liquid interface (Diaz et al., 2010), FA with a smaller mean particle size is expected to provide more surface area that will lead to a higher dissolution rate of the main precursors. Consequently, more chemical species will be available to form geopolymer and thus the compressive strength will be higher.

The density of GPC was found to be strongly influenced by the specific gravity of the FA. A regression model that explains this correlation is put forward in Section 6.1.3. The relationship between the two variables can be considered to be merely physical and attributed to the packing characteristics of FA. Changes in the void content (quantified as SG) will cause variation in the water demand to fill these voids.

The calcium content in FA is not only believed to enhance the mechanical strength but it also has a strong effect on the setting time of GPC. As it was proven by Temuujin et al. (2009) that calcium forms hydrated calcium products parallel to the formation of geopolymer. The decrease in setting time can be attributed to two mechanisms: (1) the hydrated products act as nucleation sites that accelerate the setting; and (2) the hydration of calcium consumes water, that raises the concentration of the activator solution and consequently accelerates the reaction. Although the correlation between calcium and setting time is clear, a regression model with fair accuracy could not be proposed as high variability in the setting time was encountered at low *RCaO*

values. Conversely, at moderate to high $RCaO$ values the variability in the setting time is reduced and the correlation becomes more evident. This suggests that an additional parameter, which was not taken into account, may play an important role in the setting time of GPC, particularly for FA samples with low calcium content.

Geopolymer concrete seems to possess a similar mechanical behavior to that of ordinary Portland cement concrete. The relationship between flexural and the compressive strengths of GPC can be expressed using a statistically derived equation that resemble that given by ACI 318-08 for ordinary concrete. The relationship between elastic modulus and compressive strength of GPC is similar to that of ordinary concrete; however, their relationship is linear while for ordinary concrete it follows a power curve. The elastic modulus of GPC may be better expressed as function of both density and compressive strength.

7.2. Recommendations for Future Work

The residual analysis of Eq. (3) suggested non-constant variance of the residuals, which could be a cause of concern. However, this was attributed to the fact that the majority of the compressive strength values for GPC laid in the mid to high end of the range while only a few samples exhibited mid to low values. Therefore, it is recommended that more samples that lie in the mid to low range of the compressive strength are added to the database. Alternatively, the weighted least squares technique is typically recommended to solve non-constant variance problems thus the data could be analyzed using this technique instead of OLS.

The output of Eq. (3) could be simplified by classifying FA stockpiles in a score system according to how they compare to each other in terms of potential strength of

GPC rather than predicting single values of compressive strength. This would not only simplify the output, but it would also eliminate the need to follow the same procedures and mix design to produce GPC that matches the prediction since the potential of a FA stockpile will compare to another in the same way regardless of the mix design.

An additional line of research that could improve the accuracy of Eq. (3) is the dissolution rate of crystalline phases during geopolymerization. This work was performed under the assumption that the molecules in a crystalline arrangement are inert. However, a small percentage of the crystalline phases are dissolved at different rates during the activation process, potentially forming more geopolymer. A regression model that explains the dissolution rate of crystalline phases in FA during geopolymerization could enhance the accuracy of Eq. (3).

APPENDIX A

RESULTS

Table A. 1 Chemical composition of fly ash samples

FA class	FA sample	SiO_2	Al_2O_3	SiO_2/Al_2O_3	$SiO_2+Al_2O_3$	CaO	Fe_2O_3	LOI
C	1	37.77	19.13	1.97	56.90	22.45	7.33	0.17
C	2	32.41	18.40	1.76	57.90	28.07	7.17	0.38
C	3	55.61	19.87	2.80	75.48	12.93	4.52	0.23
F	4	58.52	20.61	2.84	79.13	5.00	9.43	0.05
F	5	61.01	20.06	3.04	81.07	5.48	7.00	0.08
F	6	61.23	19.20	3.19	80.43	5.64	7.27	0.06
F	7	62.12	19.59	3.17	81.71	5.01	6.88	0.10
F	8	59.32	19.72	3.01	79.04	6.90	7.22	0.15
C	9	48.70	16.60	2.93	65.30	18.72	6.93	0.49
F	10	55.07	28.61	1.92	83.68	1.97	6.22	1.82
F	11	56.22	27.15	2.07	83.37	5.43	3.73	2.69
F	12	56.39	27.36	2.06	83.75	4.69	3.34	3.41
F	13	57.11	28.18	2.03	85.29	5.18	4.00	0.44
F	14	57.35	27.78	2.06	85.13	5.57	3.65	0.83
F	15	40.75	22.79	1.79	63.54	4.64	17.76	5.72
F	16	66.5	18.8	3.54	85.30	4.91	1.95	0.26
C	17	39.25	21.09	1.86	60.34	23.53	4.99	0.11
C	18	33.02	19.82	1.67	52.84	26.19	6.75	0.16
F	19	59.25	18.43	3.21	77.68	9.23	5.61	0.04
C	20	56.42	17.63	3.20	74.05	11.66	5.74	0.00
C	21	27.15	17.57	1.55	44.72	33.39	6.08	0.00
C	22	31.26	19.76	1.58	51.02	28.53	6.47	0.00
C	23	30.85	17.07	1.81	47.92	28.47	6.79	0.00
C	24	49.9	19.32	2.58	69.22	15.22	7.63	0.09
C	25	55.15	23.55	2.34	78.70	10.60	4.63	0.31
F	26	52.81	20.83	2.54	73.64	0.98	13.05	0.19
F	27	45.65	20.37	2.24	66.02	6.23	19.43	0.20
F	28	58.04	28.15	2.06	86.19	4.24	3.29	0.07
F	29	51.46	28.04	1.84	79.50	2.96	10.34	0.03
F	30	51.69	21.37	2.42	73.06	3.10	8.28	0.22
C	31	57.55	19.84	2.90	77.39	10.25	5.08	0.07
F	32	52.57	25.22	2.08	77.79	5.10	7.76	0.13
F	MIN	40.75	18.43	1.79	63.54	0.98	1.95	0.03
F	MAX	66.50	28.61	3.54	86.19	9.23	19.43	5.72
F	AVG	55.95	23.28	2.48	79.23	4.86	7.70	0.87
C	MIN	27.15	16.60	1.55	44.72	10.25	4.52	0.00
C	MAX	57.55	23.55	3.20	78.70	33.39	7.63	0.49
C	AVG	42.70	19.20	2.23	62.44	20.77	6.16	0.15

Table A. 2 Nomenclature of crystalline phases

Crystalline Phase	Designation
Albite($NaAlSi_3O_8$)	A
Allophane $(Al2O_3 \cdot (SiO_2)_{1.3-2} \cdot ((H_2O))_{2.5-3})$	B
Anhydrite $CaSO_4$	C
Anorthite $CaAl_2Si_2O_8$	D
Calcite $(CaCO_3)$	E
Calcium Catena Silicate $Ca(SiO_3)$	F
Cristoballite (SiO_2)	G
Dicalcium Silicate Ca_2SiO_4	H
Diopside $CaMgSi_2O_6$	I
Dolomite ($CaMg(CO_3)_2$)	J
Gehlenite $Ca_2Al_2SiO_7$	K
Grossular $(Ca_3Al_2(SiO_4)_3$	L
Gypsum $(CaSO_4 \cdot 2(H_2O)$)	M
Hematite (Fe_2O3)	N
Hydrogarnet $(CaO)_3(Al_2O_3)_1 + x(H_2O)_{6-3x}$	O
Illmenite $FeTiO_3$	P
Jadeite $NaAlSi_2O_6$	Q
Lime (CaO)	R
Magnesite $(MgCO_3)$	S
Magnetite $(Fe3O4$)	T
Merwinite $(Ca_3Mg(SiO_4)_2)$	U
Mullite $(Al_{4.5}Si_{1.5}O_{9.75})$	V
Nosean $Na_8Al_6Si_6O_{24}(SO_4)$	W
Olympite Na_3PO_4	X
Periclase (MgO)	Y
Perovskite $CaFe(Ti_2O_6)$	Z
Pseudobrookite $((Fe^{+++},Fe^{++})_2(Ti,Fe^{++})O_5)$	AA
Pyrite (FeS_2)	AB
Spinel $MgAl_2O_4$	AC
Thermonatrite $(Na_2CO_3oH_2O)$	AD
Thenardite $Na_2(SO_4)$	AE
Quartz (SiO_2)	AF
ZnO	AG
Amorphous	AH

Table A. 3 Crystallographic analysis (samples 1-5)

Phase	1		2		3		4		5	
	FA	GP	FA	GP	FA	GP	FA	GP	FA	GP
A					0.10					
B								9.30		
C			1.70							
F			0.40	0.30						
H			3.30	3.00						
I				1.50						
J					0.40					
K				0.60						
L			1.20	0.60						
N	0.30	0.30			0.30		1.30	1.30	1.90	1.90
R	0.30	0.10								
T	0.40	0.10	0.90		0.60				0.50	1.40
U	9.60	5.80								
V			1.40	0.20	1.30	2.10	6.70	7.30	10.60	5.80
W				2.20						
Y	3.20	0.20	1.80	1.10	0.40	0.50				
Z			7.90	3.60			2.10	2.00		
AA	4.20	1.40								
AF	23.10	18.30	5.10	2.50	28.30	17.30	37.00	24.80	14.90	17.00
AH	58.90	73.80	76.20	84.40	69.30	80.10	52.90	55.30	72.10	73.90

Table A. 4 Crystallographic analysis (samples 6-10)

Phase	6		7		8		9		10	
	FA	GP	FA	GP	FA	GP	FA	GP	FA	GP
E							1.60	2.70		
J							0.20	0.30		
M							1.30			
N	0.20	0.00				0.20				
S							0.90	1.50		
T	0.20	0.10	0.90	0.60	1.00	0.80				
V	5.30	2.90	6.20	3.70	5.20	4.80			25.27	14.62
Y							0.10	0.10		
AB							0.65	0.20		
AD				9.30						
AF	19.20	10.20	22.30	9.90	20.70	12.20	28.10	11.60	10.33	5.58
AG							0.10	0.10		
AH	75.10	86.80	70.60	76.50	73.10	82.00	67.05	83.50	64.40	79.80

Table A. 5 Crystallographic analysis (samples 11-15)

Phase	11		12		13		14		15	
	FA	GP	FA	GP	FA	GP	FA	GP	FA	GP
C									0.90	
N									2.40	1.60
R	2.10	0.10	1.10	0.10	1.10	0.10	0.80	0.10		
T								0.10	3.70	3.20
V	17.90	15.70	22.70	18.80	30.10	21.40	22.00	17.70		
AC									6.10	6.20
AD		3.70		4.80		3.10		3.90		
AE										3.70
AF	22.10	5.10	10.50	6.30	9.40	8.50	7.90	6.60	0.80	1.10
AH	57.90	75.30	65.70	69.90	59.40	66.80	69.20	71.60	86.10	84.20

Table A. 6 Crystallographic analysis (samples 16-20)

Phase	16		17		18		19		20	
	FA	GP	FA	GP	FA	GP	FA	GP	FA	GP
A	2.10	2.80								
C	0.30	0.20	0.30		1.00		0.40	0.30	0.30	
G	0.90									
K					3.20	1.70				
L					0.40	0.20				
P					5.80	0.20				
T	0.90	0.80			0.40	0.60	1.10	0.70	0.30	0.20
V	7.60	4.00	1.50	1.00	0.60	0.40	4.80	3.80	2.30	1.70
Y			0.80	1.00	2.80	1.10				
Z			2.50	1.00	6.00	1.40				
AD		3.90						1.50		
AF	5.30	3.70	9.00	4.60	5.60	3.10	20.90	13.40	12.20	7.90
AH	82.90	84.60	85.90	92.20	74.20	91.30	72.80	79.90	84.90	90.20

Table A. 7 Crystallographic analysis (samples 21-25)

Phase	21		22		23		24		25	
	FA	GP	FA	GP	FA	GP	FA	GP	FA	GP
C	2.10		1.40		2.30		0.20	0.30		
D	1.50									
I								2.30		
K	1.80	0.80	2.00	0.80	3.80	1.20			0.20	0.20
N							0.50	0.30		
O		9.30		5.40		1.00				
Q		3.50	0.50	2.20	1.20	2.30				
R	0.70		0.50	0.40	0.40	0.10	0.10		0.20	0.10
T								0.30	0.40	0.40
V							2.00	1.60	7.10	7.40
W		1.50		1.20		0.80				
X	1.30	2.30		0.40						
Y	1.20	0.70	1.20	0.60	2.00	0.90	0.20	0.40		
Z	9.10	0.80	5.10	1.50	6.30	2.40				
AF	3.00	3.20	3.50	3.10	4.90	2.90	10.30	6.00	8.00	9.20
AH	79.30	77.90	85.80	84.40	78.90	88.40	86.20	88.40	84.10	82.70

Table A. 8 Crystallographic analysis (samples 26-30)

Phase	26		27		28		29		30	
	FA	GP	FA	GP	FA	GP	FA	GP	FA	GP
A	0.60		0.40							
C			0.80						0.40	
E			0.20							
I		2.30	2.50	3.90		0.50				
K										
N	1.20	0.40	2.40	2.00	0.30				0.70	0.40
Q						5.50				
R					0.80				0.40	
S										
T			4.30	3.60			2.70	2.90	2.50	2.40
V	13.70	11.50	5.40	5.30	18.70	9.40	29.30	21.40	13.20	8.90
Y			0.40	0.30					0.40	0.40
AE			0.30							
AF	15.40	9.70	5.20	3.90	7.70	3.50	10.00	6.00	11.70	6.70
AH	69.10	76.10	78.40	80.70	72.50	81.10	58.00	69.70	70.00	81.20

Table A. 9 Crystallographic analysis (samples 31 and 32)

Phase	31		32	
	FA	GP	FA	GP
A			0.60	
E	2.30			
I				2.30
N			1.20	0.40
R	0.70			
T	0.90	0.80		
V	10.60	9.80	13.70	11.50
AF	12.40	9.80	15.40	9.70
AH	73.10	79.60	69.10	76.10

Table A. 10 Summary of physical properties

Sample	Particles <45 μm (%)	Calculated surface (m²/cm³)	Mean particle size (μm)	Specific gravity	Specific surface area (m²/g)
1	83.01	2.92	11.36	2.50	1.17
2	83.80	2.58	12.31	2.53	1.02
3	68.75	1.33	20.87	2.38	0.56
4	63.50	0.57	27.52	2.32	0.25
5	66.17	1.25	22.68	2.27	0.55
6	63.75	1.10	24.93	2.29	0.48
7	61.66	0.98	28.31	2.27	0.43
8	62.97	1.12	29.96	2.23	0.50
9	74.24	2.00	15.17	2.47	0.81
10	71.26	1.08	22.30	2.17	0.50
11	55.39	0.49	40.03	1.78	0.28
12	58.19	0.795	34.57	1.73	0.46
13	58.02	0.59	36.73	1.82	0.32
14	43.31	0.23	51.11	1.81	0.13
15	87.50	2.95	6.62	2.52	1.17
16	30.28	0.14	92.41	1.47	0.10
17	84.27	2.45	11.88	2.51	0.98
18	85.68	2.49	11.32	2.7	0.92
19	63.24	1.18	30.38	2.18	0.54
20	67.33	0.57	25.93	2.27	0.25
21	80.91	3.13	10.38	2.67	1.17
22	85.86	3.14	6.71	2.55	1.23
23	81.23	2.79	12.16	2.61	1.07
24	84.23	1.58	11.95	2.41	0.66
25	63.10	1.40	30.15	2.05	0.68
26	60.20	0.53	33.31	2.03	0.26
27	76.06	0.55	21.00	2.50	0.22
28	76.15	1.07	20.42	1.88	0.57
29	73.11	1.58	20.39	2.19	0.72
30	60.02	1.12	32.64	2.04	0.55
31	65.18	1.06	25.38	2.11	0.50
32	75.22	1.80	18.41	2.263	0.79

Table A. 11 Summary of fresh mix and mechanical properties of GPC samples

Fly Ash Type	Sample	w (kg/m³)	f'c (MPa)	fr (MPa)	Ec (MPa)	Poisson's Ratio	Setting Time (min)
C	1	2323	59.50	4.48	33633	0.12	1.5
C	2	2323	52.28	4.72	34377	0.12	2
C	3	2291	55.89	4.30	37108	0.17	25
F	4	2307	40.35	4.14	28599	0.14	180
F	5	2291	47.55	5.58	29475	0.16	350
F	6	2307	46.69	5.30	29358	0.14	320
F	7	2307	46.79	4.61	28517	0.13	240
F	8	2291	46.11	4.71	26455	0.12	400
C	9	2339	52.81	5.27	42878	0.13	17
F	10	2243	47.44	5.12	25635	0.14	480
F	11	1986	12.20	2.24	7040	0.17	140
F	12	1970	12.82	2.38	6812	0.10	60
F	13	1986	20.68	3.50	7960	0.08	70
F	14	1890	10.34	2.74	7460	0.10	25
F	15	2371	46.56	6.31	28744	0.15	480
F	16	1810	5.53	1.15	4619	0.12	25
C	17	2307	61.38	6.23	31447	0.18	8
C	18	2323	39.19	4.19	19064	0.22	6
F	19	2291	43.38	4.24	25607	0.13	45
C	20	2371	53.70	4.43	28910	0.15	285
C	21	2323	36.54	3.58	26972	0.13	4
C	22	2323	57.18	5.27	29448	0.19	2
C	23	2339	42.81	5.18	22567	0.22	3
C	24	2355	64.68	4.90	30806	0.15	18
C	25	2355	62.19	4.83	29896	0.14	55
F	26	1938	20.16	2.79	11273	0.14	16
F	27	2339	52.57	4.17	28089	0.14	20
F	28	2083	32.45	4.38	22808	0.13	46
F	29	2195	23.36	2.52	13176	0.12	75
F	30	2131	22.68	3.94	12314	0.14	11
C	31	2163	36.24	3.25	21456	0.14	17
F	32	2243	36.80	4.56	24725	0.14	47
F	MINIMUM	1810	5.53	1.15	4619	0.08	11
	MAXIMUM	2371	52.57	6.31	29475	0.17	480
	AVERAGE	2157	32.34	3.91	19403	0.13	159
C	MINIMUM	2163	36.24	3.25	19064	0.12	2
	MAXIMUM	2371	64.68	6.23	42878	0.22	285
	AVERAGE	2318	51.88	4.66	29889	0.16	34

Table A. 12 Chemical composition of crystalline phases

Crystalline phase	SiO$_2$	Al$_2$O$_3$	CaO	Fe$_2$O$_3$
A	67.39	20.35	1.07	-
B	34.7	45.29	-	-
C	-	-	41.19	-
D	44.4	35.84	19.2	-
E	-	-	56.03	-
F	51.72	-	48.28	-
G	100.00	-	-	-
H	31.5	2.1	63.5	0.9
I	55.49	-	25.9	-
J	-	-	30.41	-
K	21.91	37.18	40.9	-
L	40.02	22.64	37.35	-
M	-	-	32.57	-
N	-	-	-	100
O	21.75	24.61	40.6	-
P	-	-	-	47.35
Q	58.61	22.38	-	3.89
R	-	-	100.00	-
T	-	-	-	100
U	36.56	-	51.18	-
V	28.21	71.79	-	-
W	35.61	30.21	-	-
Z	-	-	41.25	-
AA	-	-	-	69.83
AC	-	71.67	-	-
AF	100	-	-	-

Table A. 13 Reactive content in fly ash samples

Class	Sample	RSiO$_2$	RAl$_2$O$_3$	RCaO
C	1	11.16	19.13	17.24
C	2	25.19	17.05	21.37
C	3	26.88	18.92	12.81
F	4	19.63	15.80	4.13
F	5	43.12	12.45	5.48
F	6	40.53	15.40	5.64
F	7	38.07	15.14	5.01
F	8	37.15	15.99	6.90
C	9	20.60	16.60	17.34
F	10	37.61	10.47	1.97
F	11	29.07	14.30	3.33
F	12	39.49	11.06	3.59
F	13	39.22	6.57	4.08
F	14	43.24	11.99	4.77
F	15	39.95	18.42	4.27
F	16	56.74	12.92	4.76
C	17	29.83	20.01	22.38
C	18	26.39	18.11	21.84
F	19	37.00	14.98	9.07
C	20	43.57	15.98	11.54
C	21	23.09	16.36	27.05
C	22	27.03	18.90	24.53
C	23	24.41	15.39	22.97
C	24	39.04	17.88	15.04
C	25	45.10	18.38	10.32
F	26	33.14	10.87	0.97
F	27	37.27	16.41	5.14
F	28	45.06	14.73	3.44
F	29	33.19	7.01	2.96
F	30	36.27	11.89	2.54
C	31	42.16	12.23	8.26
F	32	32.90	15.26	5.09

APPENDIX B

STATISTICAL PROGRAMMING

R code of approach one

```
# LEAPS

data(gpcfinal)
gpcfinal
attach(gpcfinal)
x<-as.matrix(gpcfinal[,c(6:9,12,14)])
y<-as.matrix(gpcfinal[,c(16)])
library(leaps)
leaps( x, y, names=colnames(x),nbest=1, method="adjr2")
model1 <- lm(fc~RSiO2+RAl2O3+RCaO+d50+LOI)
summary(model1)
anova(model1)
library (car)
vif(model1)
library(MPV)
PRESS(model1)

opar <- par()
par(mfcol = c(2,2))
windowsFonts(A=windowsFont("Times New Roman"))
plot(model1, which= 1,
main="Residual analysis and Normal probability plot of model 1",family="A")
plot(model1, which= 2,family="A")

windowsFonts(A=windowsFont("Times New Roman"))
plot(fitted(model1),fc,ylab="Experimental compressive strength (MPa)",
xlab="Predicted compressive strength (MPa)", xlim=c(0,70), ylim=c(0,70),
main="Error of model 1",family="A")
segments(0,0,70,70)
MSE=sum((as.matrix(fc)-fitted(model1))^2)/18
MSE

#Validation using new data

data(gpcvalid)
gpcvalid
attach(gpcvalid)
predict.lm(model1,gpcvalid)
validation<-predict.lm(model1,gpcvalid)

windowsFonts(A=windowsFont("Times New Roman"))
plot(validation, fc, ylab="Experimental compressive strength (MPa)",
xlab="Predicted compressive strength (MPa)", xlim=c(0,70), ylim=c(0,70),
main="Validation of model 1 using new data",family="A")
```

```
segments(0,0,70,70)
detach(gpcvalid)
```

```
#Cross-Validation
```

```
library(DAAG)
windows()
opar <- par()
par(mfcol = c(2,2))
windowsFonts(A=windowsFont("Times New Roman"))
main="Cross-Validation of Model 1"
CVlm( df=gpcfinal, model1, 2)
CVlm( df=gpcfinal, model1, 3)
CVlm( df=gpcfinal, model1, 4)
CVlm( df=gpcfinal, model1, 5)
```

R code of approach two

```
# LASSO
```

```
data(gpcfinal)
gpcfinal
attach(gpcfinal)
library(lars)
trnx<-as.matrix(gpcfinal[,c(6:9,12,14)])
trny<-as.matrix(gpcfinal[,c(16)])
```

```
library(lars)
model2<-lars(trnx,trny, normalize=F,intercept=TRUE,trace=TRUE)
summary(model2)
coef(model2, intercept=TRUE, mode="step")
coef(model2,s=8,intercept=TRUE,model="step")
predict.lars(model2, newx=trnx, s=8,type = c("fit"), intercept=TRUE, mode="step")
```

```
data(lassofit)
lassofit
attach(lassofit)
MSE=sum((as.matrix(lassofit)-trny)^2)/18
MSE
windows()
opar <- par()
par(mfcol = c(2,2))
windowsFonts(A=windowsFont("Times New Roman"))
plot(as.matrix(lassofit), trny,main="Linearization of model 2",
xlab="Predicted compressive strength (MPa)",
```

```
ylab="Experimental compressive strength (MPa)",
xlim=c(0,70), ylim=c(0,70),family="A")
segments(0,0,70,70)
```

```
# Validating using new data
```

```
data(gpcvalid)
gpcvalid
attach(gpcvalid)
tstx<-as.matrix(gpcvalid[,c(6:9,12,14)])
tsty<-as.matrix(gpcvalid[,c(16)])
predict.lars(model2, newx=tstx, s=8,type = c("fit"), intercept=TRUE, mode="step")
data(lassopredicted)
lassopredicted
attach(lassopredicted)
plot(as.matrix(lassopredicted), tsty,main="Validation of model 2 using new data",
xlab="Predicted compressive strength (MPa)",
ylab="Experimental compressive strength (MPa)",
xlim=c(0,70), ylim=c(0,70),family="A")
segments(0,0,70,70)
```

```
RES=trny-as.matrix(lassofit)
plot(as.matrix(lassofit),RES,main="Residual vs. Fitted",
xlab="Fitted values",ylab="Residuals",
xlim=c(0,70), ylim=c(-20,20),family="A")
segments(0,0,70,0,lty=2)
```

```
SRES=RES/sqrt(MSE)
qqnorm(SRES,xlab="Theoretical quantiles",ylab="Standardized residuales",family="A")
segments(-2,-2,2,2, lty=2)
```

R code of approach three

```
#ELASTIC NET
```

```
data(gpcfinal)
attach(gpcfinal)
trnx<-as.matrix(gpcfinal[,c(6:9,12,14)])
trny<-as.matrix(gpcfinal[,c(16)])
library(glmnet)
lmbda=seq(900, 0.01, length.out=10000)
fit1=cv.glmnet(trnx, trny, standardize=F,
lambda=lmbda , nfolds=6, dfmax=10, alpha=.9)
coef(fit1,lambda="lambda.min")
```

```
data(gpcvalid)
```

```
attach(gpcvalid)
tstx<-as.matrix(gpcvalid[,c(6:9,12,14)])
tsty<-as.matrix(gpcvalid[,c(16)])

windows()
opar <- par()
par(mfcol = c(2,2))
windowsFonts(A=windowsFont("Times New Roman"))

MSE=sum((trny-as.matrix(predict(fit1,newx=trnx,lambda="lambda.min")))^2)/18
MSE
plot(predict(fit1,newx=trnx,lambda="lambda.min"), trny,
main="Linearization of model 3",
xlab="Predicted compressive strength (MPa)",
ylab="Experimental compressive strength (MPa)",
xlim=c(0,70), ylim=c(0,70),family="A")
segments(0,0,70,70)
plot(predict(fit1,newx=tstx,lambda="lambda.min"),
tsty, main="Validation of model 3 using new data",
xlab="Predicted compressive strength (MPa)",
ylab="Experimental compressive strength (MPa)",
xlim=c(0,70), ylim=c(0,70),family="A")
segments(0,0,70,70)

RES=trny-predict(fit1,newx=trnx,lambda="lambda.min")
plot(predict(fit1,newx=trnx,lambda="lambda.min"),
RES,main="Residual vs. Fitted", xlab="Fitted values",ylab="Residuals",
xlim=c(0,70), ylim=c(-20,20),family="A")
segments(0,0,70,0,lty=2)

SRES=RES/sqrt(MSE)
qqnorm(SRES,xlab="Theoretical quantiles",ylab="Standardized residuales")
segments(-2,-2,2,2, lty=2)
```

R code for the practical approach

```
data(gpcfinal)
gpcfinal
attach(gpcfinal)
library(lars)
trnx<-as.matrix(gpcfinal[,c(2:4,6,12,14)])
trny<-as.matrix(gpcfinal[,c(16)])
library(HH)
vif(gpcfinal[,c(2:4,6,12,14)])

library(lars)
```

```
model2<-lars(trnx,trny, normalize=F,intercept=TRUE,trace=TRUE)
summary(model2)
coef(model2, intercept=TRUE, mode="step")
coef(model2,s=5,intercept=TRUE,model="step")
predict.lars(model2, newx=trnx, s=4,type = c("fit"), intercept=TRUE, mode="step")

ft<-data.frame(predict.lars(model2, newx=trnx, s=5,type = c("fit"),
intercept=TRUE, mode="step"))
lassofit<-ft[,c(4)]

MSE=sum((as.matrix(lassofit)-trny)^2)/18
MSE
windows()
opar <- par()
par(mfcol = c(2,2))
windowsFonts(A=windowsFont("Times New Roman"))
plot(as.matrix(lassofit), trny,main="Linearization of model 2",
xlab="Predicted compressive strength (MPa)",
ylab="Experimental compressive strength (MPa)",
xlim=c(0,70), ylim=c(0,70),family="A")
segments(0,0,70,70)

data(gpcvalid)
gpcvalid
attach(gpcvalid)
tstx<-as.matrix(gpcvalid[,c(2:4,6,12,14)])
tsty<-as.matrix(gpcvalid[,c(16)])
predict.lars(model2, newx=tstx, s=5,type = c("fit"), intercept=TRUE, mode="step")

ft2<-data.frame(predict.lars(model2, newx=tstx, s=5,type = c("fit"),
intercept=TRUE, mode="step"))
lassopredicted<-ft2[,c(4)]

plot(as.matrix(lassopredicted), tsty,main="Validation of model 2 using new data",
xlab="Predicted compressive strength (MPa)",
ylab="Experimental compressive strength (MPa)",
xlim=c(0,70), ylim=c(0,70),family="A")
segments(0,0,70,70)

RES=trny-as.matrix(lassofit)
plot(as.matrix(lassofit),RES,main="Residual vs. Fitted",
xlab="Fitted values",ylab="Residuals",
xlim=c(0,70), ylim=c(-20,20),family="A")
segments(0,0,70,0,lty=2)
data.frame(trny,lassofit,RES)
RESP=tsty-as.matrix(lassopredicted)
```

```
data.frame(tsty, lassopredicted, RESP)
SRES=RES/sqrt(MSE)
qqnorm(SRES,xlab="Theoretical quantiles",ylab="Standardized residuales",family="A")
segments(-2,-2,2,2, lty=2)
```

APPENDIX C

IMAGES OF MECHANICAL TESTING
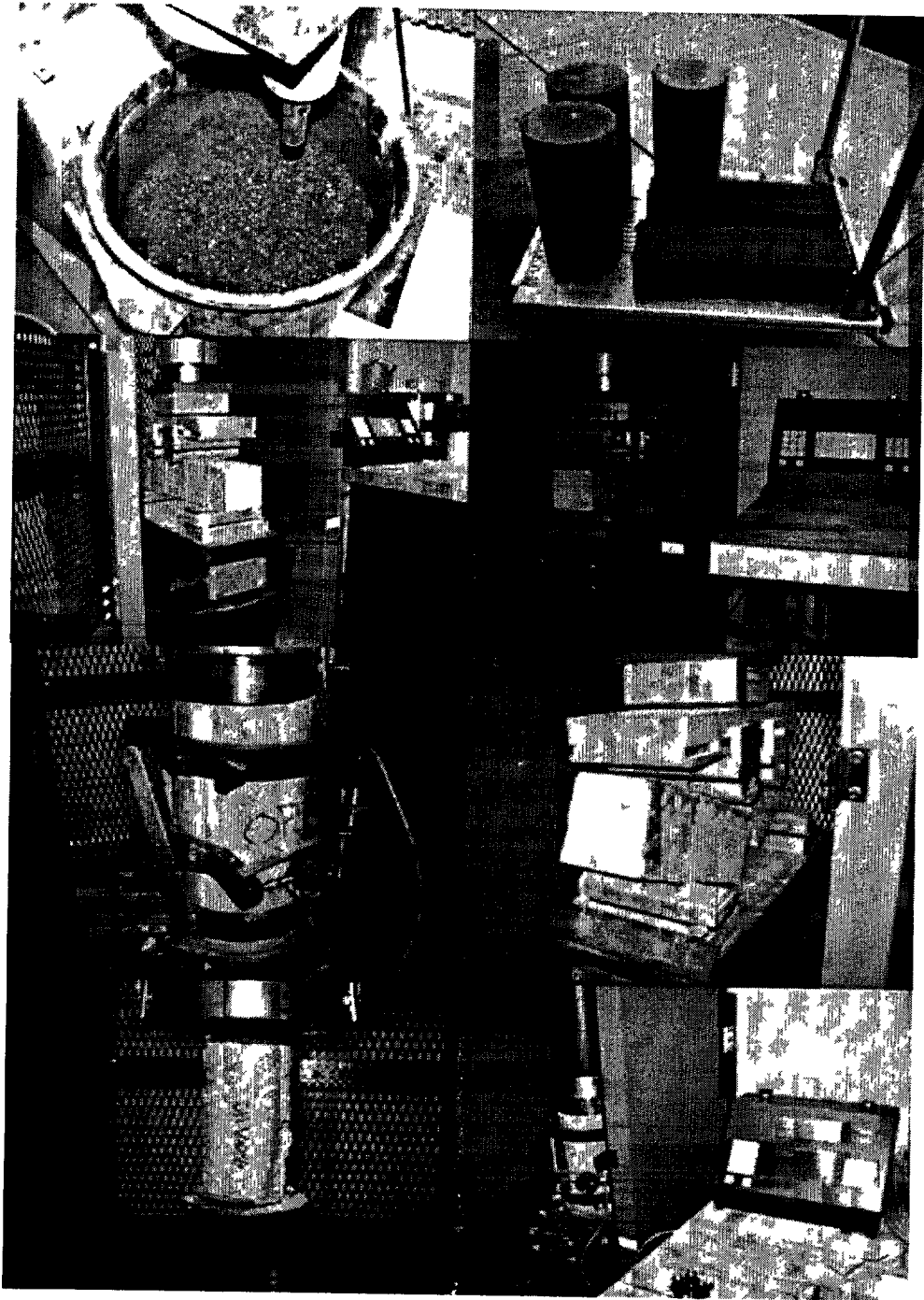
Figure C.1 Images of the mechanical testing

REFERENCES

Allouche, E. N.; Montes, C.; Diaz Loya, E. I.; and Vernon, G., "Applications of geopolymer concrete in the rehabilitation of wastewater concrete structures," NASTT No-Dig Conference and Exhibition, April 2008, Dallas, TX.

American Coal Ash Association, "2009 Coal combustion product (CCP) production and use survey," 2010 [online]. Available from: http://acaa.affiniscape.com/display common.cfm?an=1&subarticlenbr=3, [Accessed: January 5, 2011].

American Concrete Institute, "Building Code requirements for structural concrete and commentary," 2008.

Breiman, L., "Heuristics of instability and stabilization in model selection," *Annals of Statistics*, vol. 24, 1996, 2350–2383.

Chindraprasirt, P.; Chareerat, T.; Hatanaka, S.; and Cao, T., "High-strength geopolymer using fine high-calcium fly ash," *J. of Mat. in Civ. Eng.*, vol. 23, 2011, article in press (doi:10.1061/(ASCE)MT.1943-5533.0000161).

Davidovits, J., "Carbon-dioxide green-house warming: What future for Portland cement," Emerging technologies symposium on cement and concretes in the global environment, Portland Cement Association, Chicago, Ill., 1993, 21.

Davidovits, J., "Geopolymers: inorganic polymeric new materials," *J. of Thermal Analysis*, vol. 37, 1991, 1633–1656.

Davidovits, J., "Chemistry of geopolymeric systems, terminology," Geopolymer International Conference, France, 1999.

De Silva, P.; Sagoe-Crenstil, K.; and Sirivivatnanon, V., "Kinetics of geopolymerization: Role of Al_2O_3 and SiO_2," *Cem. and Concrete Res.*, vol. 37, 2007, 512-518.

Dewan, S., "Coal ash spill revives issue of its hazards," New York Times, December 24, 2008.

Diamond, S., "On the glass present in low-calcium and in high-calcium fly ashes," *Cem. and Concrete Res.*, vol. 13, 1983, 459-464.

Diaz, E. I., and Allouche, E. N., "Recycling of fly ash into geopolymer concrete: Creation of a database," Green Technologies Conference, 2010 IEEE. 2010, 1-7.

Diaz, E. I.; Allouche, E. N.; and Eklund, S., "Factors affecting the suitability of fly ash as source material for geopolymers," *Fuel*, vol. 89, 2010 992-996.

Environmental Protection Agency (EPA), "Coal combustion residual-proposed rule," www.epa.gov, January 10, 2011.

Fernandez-Jimenez, A., and Palomo, A., "Characterization of fly ashes: Potential reactivity as alkaline cements," *Fuel*, vol. 82, 2003, 2259-2265.

Fernández-Jiménez, A. M.; Palomo, A.; and López-Hombrados, C., "Engineering properties of alkali-activated fly ash concrete," *ACI Materials J.*, vol. 103, 2006, 106-112.

Fernandez-Jimenez, A., and Palomo, A., "Alkaline activation of fly ashes; Manufacture of concrete not containing Portland cement," International RILEM Conference on the Use of Recycled Materials in Building and Structures, 2004.

Gao, Y. M.; Shim, H. S.; Hurt, R. H.; and Suuberg, E. M., "Effects of carbon on air entrainment in fly ash concrete: the role of soot and carbon black," *Energy Fuels*, vol. 11 (2), 1997, 457-462.

Hardjito, D.; Wallah, S. E.; Sumajouw, D. M. J.; and Rangan, B. V., "On the development of fly ash-based geopolymer concrete," *ACI Materials J.*, vol. 101 (6), 2004, 467-472.

Hasti, T., and Efron, B., "Least angle regression, LASSO and stagewise regression (package LARS)," 2007 [online]. Available from: http://cran.r-project.org/web/packages/lars/lars.pdf [Accessed: February 17th, 2011].

Hill, R. L., and Folliard, K. J., "The impact of fly ash on air-entrained concrete," *Concrete InFocus*, Fall 2006, 71-72.

Hoerl, A. E., and Kennard, R. W., "Ridge regression: Applications to nonorthogonal problems," *Technometrics*, vol. 12 (1), 1970, 69-82.

Hunger, M., and Brouwers, H. J. H., "Flow analysis of water-powder mixtures: Application to specific surface area and shape factor," *Cem. and Concrete Composites*, vol. 31, 2009, 39-59.

Kosmatka, S.; Kerkhoff, B.; and Panarese, W., "Design and control of concrete mixes," Portland Cement Association, 14th ed., 2009.

Kutner, M.; Nachtsheim, C.; and Neter, J., "Applied linear regression models," 4th Ed., Macgraw-Hill Irwin, 2004.

Li, Q., and Lin, N., "The Bayesian elastic net," *Bayesian Analysis J.*, vol. 5 (1), 2010, 151-170.

Lumley, T., "Regression subset selection (package leaps)," 2009 [online]. Available from: http://www.cran.r-project.org/web/packages/leaps/leaps.pdf. [Accessed: February 17th 2009].

MacGregor, J. G., and Wight, J. K., "Reinforced concrete: Mechanics and design," 4th Ed., Prentice Hall, New Jersey, 2005,74-86.

Martin, M.; Renault, M.; Jezequel, P. H.; and Garcia, E., "Mixability and particle size distribution criteria: Study on model materials," *Powder Technology*, vol. 190 (1-2), 36-40.

Montgomery, D. C.; Peck, E. A.; and Vining, G. G., "Introduction to linear regression analysis," 4th Ed., Wiley-Interscience, New Jersey, 2006, 122-153.

Pade, C., and Guimaraes, M., "The CO_2 uptake of concrete in a 100 year perspective," *Cem. and Concrete Res.*, vol. 37 (9), 2007, 1348-1356.

Palomo, A.; Grutzeck, M. W.; and Blanco, M. T., "Alkali-activated fly ashes a cement for the future," *Cem. and Concrete Res.*, vol. 29, 1999, 1323-1329.

Potgieter-Vermaak, S. S.; Potgieter, J. H.; and van Grieken, R., "The application of Raman spectrometry to investigate and characterize cement, Part I: A review," *Cem. and Concrete Res.*, vol. 36, 2006, 656-662.

Provis, J. L.; Duxson, P.; and van Deventer, J. S. J., "The role of particle technology in developing sustainable construction materials," *Advance Powder Technology*, vol. 21 (1), 2010, 2-7.

Provis, J. L.; Duxson, P.; Van Deventer, J. S. J.; and Lukey, G. C., "The role of mathematical modeling and gel chemistry in advancing geopolymer technology," *Chem. Eng. Res. and Design*, vol. 83 (7), 2005, 853-860.

Provis, J. L., and van Deventer, J. S. J., "Geopolymerization kinetics. 1. *In situ* energy-dispersive x-ray diffractometry," *Chem. Eng. Science*, vol. 62, 2007, 2309-2317.

Sofi, M.; van Deventer, J. S. J.; Mendis, P. A.; and Lukey, G. C., "Engineering properties of inorganic polymer concretes (IPCs)," *Cem. and Concrete Res.*, vol. 37 (2), 2007, 251-257.

Temuujin, J.; van Riessen, A.; and Williams. R., "Influence of calcium compounds on the mechanical properties of fly ash geopolymer pastes," *J. Hazard. Mater.*, vol. 167, 2009, 82-88.

Tibshirani, R. "Regression shrinkage and selection via the LASSO," *J. R. Statistic Soc.*, vol. 58 (1), 1996, 267-288.

van Deventer, J. S. J.; Provis, J. L.; Duxson, P.; and Brice, D. G., "Chemical research and climate change as drivers in the commercial adoption of alkali activated materials," *Waste and Biomass Valorization*, vol. 1(1), 2010, 145-155.

van Jaarsveld, J. G. S.; van Deventer, J. S. J.; and Lukey, G. C., "The effect of composition and temperature on the properties of fly ash- and kaolinite-based geopolymers," *Chem. Eng. J.*, vol. 89, 2002, 63-73.

van Jaarsveld, J. G. S.; van Deventer, J. S. J.; and Lukey, G. C., "The characterization of source materials in fly ash-based geopolymers," *Materials Letters*, vol. 57, 2003, 1272-1280.

Weil, M.; Jeske, U.; Dombrowski, K.; and Buchwald, A., "Sustainable design of geopolymers - Evaluation of raw materials by the integration of economic and environmental aspects in the early phases of material development," Advances in Life Cycle Engineering for Sustainable Manufacturing Businesses 2007, 1st Ed., Springer, Tokyo, vol. 3(4), 2007, 279-283.

World Business Council for Sustainable Development, "Cement technology roadmap 2009," 2009 [online]. Available from: www.wbcsd.org/DocRoot/mka1EKor6mq LVb9w903o/WBCSD-IEA_CementRoadmap.pdf [Accessed: March 3, 2011].

Xu, H., and van Deventer, J. S. J., "The Geopolymerization of Alumino-Silicate Minerals," *Int. J. of Mineral Processing*, vol. 59 (3), 2000, 247-266.

Zou, H., and Hastie, T., "Regularization and variable selection via the elastic net," *J. R. Statist. Soc.*, vol. 67 (2), 2005, 301–320.

Zuda, L., and Cerny, R., "Measurement of linear thermal expansion coefficient of alkali-activated aluminosilicate composites up to 1000°C," *Cem. and Concrete Composites*, vol. 31 (4), 2009, 263-267.